2. Numerical Effort

2.1 Numerical Simulation of Three Dimensional Oscillatory Marangoni Flow in Adiabatic Cylindrical Half-Zone Liquid Bridges

N. Imaishi

Kyushu University

Numerical Simulation of Three Dimensional Oscillatory Marangoni Flow in Adiabatic Cylindrical Half-Zone Liquid

Shouichi Yasuhiro and Nobuyuki Imaishi*

Institute of Advanced Material Study
Kyushu University
Kasuga, Fukuoka, 816-8580, Japan

Shinich Yoda
NASDA

ABSTRACT

Unsteady three dimensional numerical simulations were conducted for oscillatory Marangoni convection in half zone liquid bridges (radius a and length L) with non-deformable cylindrical surface by means of a finite difference scheme. Temperature and velocity fields in an adiabatic liquid bridge of Pr=1 fluid with four different aspect ratios As (=L/a) =0.75, 1.0, 1.33 and 1.60, and also in liquid bridge of Pr=0.02 with As=1.8, under various Marangoni numbers (Ma). The results for a fluid of Pr=1.0 indicated the transition from an axisymmetric to 3-D flow is accompanied by traveling hydrothermal waves in high Prandtl number fluid with different azimuthal wave numbers (m=1, 2 , 3 and 4) and two types of oscillation, *i.e.*, *pulsating* and *rotating* oscillations, depending on the Marangoni number and the flow structure previously experienced. In low Prandtl number fluid liquid bridges, however, the first instability bring out a steady 3-D flow, as linear stability analyses predicted. At larger Marangoni numbers, there occurs a second instability to initiate a three dimensional oscillatory flow which does not indicate distinguishable rotating motion. The present simulations also revealed that the 3-D disturbances grow exponentially with time. And the growth rate constants were determined as a function of the Marangoni number. The resultant critical Marangoni number values show good agreements with those predicted by linear stability analysis and previous numerical simulations.

1. INTRODUCTION

Thermocapillary (Marangoni) convection occurs in many crystal growth and other technical processes. Beside the full zone liquid bridges in practical FZ processes, the half zone liquid bridge of length L and radius a confined between two differentially heated isothermal solid disks becomes a typical model for the study of thermocapillary flows, their stability and their bifurcation, the so-called half-zone problems. Experiments with this simple geometry revealed that the basic thermocapillary flow in a half-zone is steady and axisymmetrically two dimensional if the temperature difference

between the two disks is sufficiently small. However, the basic steady axisymmetric flow becomes unstable and three dimensional (3-D) flow arises when the Marangoni number exceeds a certain threshold value. Many features of the super-critical flow, such as the azimuthal wave number m and the type of oscillation, i.e. *pulsating* or *rotating*, have been reported at different aspect ratios $As=L/a$ and the Marangoni numbers, Ma, for various fluids [1-7].

To date, several numerical investigations of the half-zone problem have become available. Rupp *et al.* [8] performed a series of fully 3-D simulation for an aspect ratio As=1.2 by means of the finite difference method and found the azimuthal wave number m=2 to be the most dangerous mode for a wide range of Prandtl number ($Pr=\nu/\alpha$). Neitzel *et al.* [9] determined the critical Marangoni number (Ma_{cE}), below which the axisymmetric flow is absolutely stable, by means of energy stability analysis for a half-zone of a fluid with Pr=1.0 and Bi=0.3 (Bi : Biot number) with various aspect ratios and found the critical Marangoni number and the most dangerous azimuthal wave number depend on the aspect ratio. Later, Neitzel *et al.*[10] determined the critical Marangoni number (Ma_{cL}) above which three dimensional disturbances can grow. Wanschura *et al.* [11]and Chen *et al.*[12] reported Ma_{cL} and some spatial structures of the 3-D disturbances at their neutral mode, for a wide range of Pr by linear stability analysis. These linear stability analyses[10-12] predict that the instability at large Pr is oscillatory, however, it is stationary at small Pr (Pr<0.1). Levenstam *et al.*[13] performed fully non-linear 3-D numerical simulations for half-zone for Pr=0.01 and recognized that the first instability is stationary as predicted by linear stability analysis and also that the second bifurcation to an oscillatory flow occurs at much higher Marangoni numbers. Savino and Monti [14] reported 3-D numerical simulations for liquid bridges of Pr=30, As=2.0 and Pr=74, As=3 showed good agreement with their microgravity experiments. Imaishi and Yasuhiro[15,16] performed series of 3-D numerical simulation for Pr=1.02 fluid by means of a finite difference method with non-uniform grid points and showed pulsating and rotating modes with m=1, 2, 2 and 3 for As=1.60, 1.33, 1.00 and 0.75, respectively. The results explained the multi-morphological features of the 3-D Marangoni flow in liquid bridge which have been well known by experiments and by linear stability analyses. Castagnolo and Carotenuto[17] performed 3-D simulations for Pr=1.0, As=1.0 and for Pr=32, As=1 and 2. They obtained a critical Marangoni number value of 2488 for the case of As=1.0 and Pr=1.0, which was very close to Ma_c=2539 predicted by linear stability analysis. In those simulations for high Prandtl number fluids, the oscillatory flow started as a *pulsating* oscillation and then transition occurred to a *rotating* oscillation.

Despite these numerical results, the understanding of the phenomena seems yet incomplete and growth rates of 3-D disturbances are still unknown. In the previous simulations of the present authors [15,16], the growth rate of 3-D disturbance was enhanced by applying non-axisymmetric heat exchange with ambient gas for a short time. This trick was necessary to reduce computing time on an EWS at that time. In the present paper, a series of numerical experiments on the time evolution of 3-D oscillatory flows in an adiabatic half-zone with non-deformable cylindrical surface under microgravity

were performed so as to obtain a deeper understanding of the flow structure and the growth process of 3-D steady and oscillatory flows and further to obtain, 1) information on the reliability of linear stability analysis, 2) correlation of growth rate with Marangoni number, 3) an explanation of the multi-morphological characteristics of 3-D flows, and 4) 3-D flow characteristics.

2. MATHEMATICAL MODEL

A half-zone liquid bridge with a non-deformable cylindrical surface of radius a is sustained between two differentially heated discs in microgravity circumstance as shown in **Fig. 1.** The distance between two discs is L and the temperature difference is ΔT. The thermophysical properties of the liquid are assumed constant except for the temperature dependency of surface tension ($\sigma_T = \partial \sigma / \partial T$). The liquid surface is assumed to be adiabatic. The initial condition assumes all quiescent liquid at T_c. From $\tau=0$, the lower disc temperature is instantaneously raised and kept at $T_h=T_c+\Delta T$, and the upper colder disc temperature is maintained at T_c.

The fundamental equations, boundary and initial conditions are described in non-dimensional forms as follows:

Continuity equation: $\nabla \cdot \boldsymbol{U} = 0$ (1)

Momentum equation: $\partial \boldsymbol{U} / \partial \tau + (\boldsymbol{U} \cdot \nabla)\boldsymbol{U} = -Pr \nabla P + Pr \nabla^2 \boldsymbol{U}$ (2)

Energy equation: $\partial \Theta / \partial \tau + (\boldsymbol{U} \cdot \nabla)\Theta = \nabla^2 \Theta$ (3)

Initial conditions: $\boldsymbol{U} = 0, \quad \Theta = -0.5 \qquad \tau \le 0$ (4)

Boundary conditions: $U_{(R,\theta,0)} = U_{(R,\theta,1)} = 0, \quad \Theta_{(R,\theta,0)} = +0.5, \quad \Theta_{(R,\theta,1)} = -0.5 \quad (\tau > 0)$ (5)

at $R=1$ $\partial \Theta / \partial R = 0, \quad \partial U_Z / \partial R = -Ma \, \partial \Theta / \partial Z,$ (6)

$R^2 \partial (U_\theta / R) / \partial R = -Ma \, \partial \Theta / \partial \theta, \quad U_R = 0$ (7)

The dimensionless parameters arising are the Prandtl, the Marangoni and the Biot numbers defined as $Pr = \nu/\alpha$ and $Ma = -\sigma_T \Delta T a / \mu\alpha$.

And the non-dimensional variables are defined as;

$\{R, Z\} = \{r/a, z/a\}, \; P = p a^2/(\alpha\mu), \; U = ua/\alpha, \; \Theta = (T - T_m)/\Delta T, \; \tau = t\alpha/a^2$ (8)

where $T_m = (T_h + T_c)/2$, $\alpha = \lambda / c_p \rho$ (thermal diffusivity), u: velocity, p: pressure, c_p: heat capacity, ρ: density, λ: thermal conductivity, μ: viscosity, and ν: kinematic viscosity.

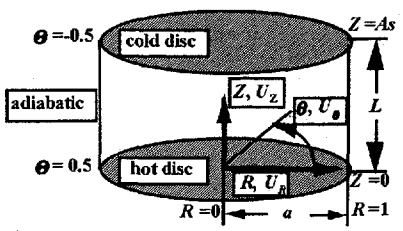

Fig.1 System coordinates.

3. NUMERICAL METHOD

Using cylindrical coordinates, these equations are discretized by a finite difference method with a modified central difference treatment for the convective term [18] and non-uniform staggered grids. The radial velocities on the central axis were calculated by means of the method of Ozoe *et al.*[19]. The HSMAC scheme [20] was used to proceed time evolution of velocity and pressure. The calculations were run on an MPU of the Fujitsu VPP700 at the Computer Center of Kyushu University. Non-uniform grids were adopted to increase the resolution. The number of grid points is listed in Table 1 together with the other conditions. Time step $\Delta\tau$ was chosen between 5×10^{-7} and 2×10^{-6} for Pr=1 and between 1×10^{-6} and 5×10^{-6} for Pr=0.01. A two dimensional simulation code with the same scheme and 2-D grids was run in order to obtain a 2-D solution under the same conditions. For a liquid bridge of Pr=1 fluid, thermophysical properties of molten KCl were adopted here as; $\alpha=7.2\times10^{-7}$ [m^2/s], $\lambda=0.99$ [W/(m·K)], $\mu=1.13$ [mPa·s], $\nu=7.41\times10^{-7}$ [m^2/s], $\sigma_T=-7.1\times10^{-5}$ [N/(m·K)] and $Pr=1.02$. Thus $\Delta\tau=1$ corresponds to 13 seconds for a real system in which a is 3.0mm. For Pr=0.01 liquid bridge, thermophysical properties of molten silicon were adopted as; $\alpha=2.5\times10^{-5}$ [m^2/s], $\lambda=64$ [W/(m·K)], $\mu=0.62$ [mPa·s], $\nu=2.5\times10^{-7}$ [m^2/s], $\sigma_T=-1.0\times10^{-4}$ [N/(m·K)] and $Pr=0.01$. Thus $\Delta\tau=1$ corresponds to 1 second for a real system in which a is 5.0mm.

The local and average Nusselt numbers are defined on both solid walls as

$$Nu=|\partial\Theta/\partial Z| \text{ and } \overline{Nu}=\int_0^{2\pi}\int_0^1 R\,|\partial\Theta/\partial Z|\,dR d\theta/2\pi \tag{9}$$

In order to express the motion of fluid elements, trajectories of infinitesimal tracer particles were calculated during the unsteady calculation by using the Euler method. The tracer particles are assumed to follow the local velocity of fluid without any slip velocity.

4. Code validation

For the whole range of the Marangoni number adopted in this work, the 2-D unsteady code gives axisymmetric steady solutions. The present 3-D code also gives axisymmetric steady solution which is indistinguishable from the 2-D solution, if the Marangoni number is smaller than the corresponding critical value which will be described later. And even beyond the critical Marangoni number, the 3-D code gives practically the same results with those of the 2-D code during the initial transient stage except for the growing 3-D disturbances, as far as their oscillation amplitudes are very small. The present discretization method provides very good heat balance (within 0.6%) on both solid disks. This is also true for all 3-D calculations, indicating the reliability of the present 2-D and 3 D numerical codes. Further, as will be discussed in detail later in section 4.3, the critical Marangoni number value fall very close (in few percents) to those of linear stability analyses and also very close to the first and the second critical Marangoni numbers given by Levenstam et al. for Pr=0.01 with As=1.0. And our 3-D simulation results could semi-quantitatively explain the experimentally observed characteristics

of 3-D oscillatory thermocapillary flows of Ref..2, such as the oscillation frequency and the flow pattern, as have been discussed in our previous paper[16]. These results support the validity of the present 3-D code for both low and medium Prandtl number fluids.

5. Case studies with fluid of Pr=1

5.1 As=1.0

5.1.1 *Ma*=4440

For all values of Marangoni numbers used here, the 2-D code gives axisymmetric steady solutions, however, 3-D simulation gives time evolution of 3-D disturbance. **Fig.2** shows time evolution of the axial and the azimuthal velocities at point A (R=1, θ=3π/4, Z=0.5) and B (R=1, θ=π, Z=0.5), the local temperatures at points A, B, C(R=0.5, θ=3π/4, Z=0.5) and D (R=0.5, θ=π, Z=0.5), a local Nusselt number at point E (R=0.5, θ=π, Z=0) and the spatially averaged non-dimensional heat fluxes (Nu) on the end plates. At the initial transient stage, surface velocity U_z shows a large overshoot due to the step-wise temperature increase at τ=0. During a time span of about $\Delta\tau$=0.75 after the overshoot, a steady and axisymmetric flow pattern was established and appears to be stable. At this stage, the velocity and temperature distributions are indistinguishable from those of 2-D solution on a linearly scaled plot. As the plot of $\ln(U_\theta)$ in Fig.2-b reveals, however, some periodic azimuthal motions, although very weak, have been created within the initial transient stage. This indicates the 2-D steady axisymmetric flow in a liquid bridge with As=1.0 can not sustain itself stable in a 3-D system at Ma=4440. It should be noted that we did not give any structured initial disturbances as an initial condition. The 3-D disturbances are caused by unavoidable small numerical errors in calculations. The slope of the line connecting the peak velocities corresponds to the growth constant β by which linear stability analysis expresses time evolution of a quantity X in the following form,

$$X_{(t)} = F_{X(R,Z)} \exp((\beta + i\omega)\tau) \sin(m\theta) \qquad (10)$$

where $\omega = 2\pi f a^2/\alpha$ is the nondimensional expression of the frequency of oscillation f, m the azimuthal wave number, and F_X the eigen-function for the quantity.

As mentioned above, the 3-D disturbances are automatically self-excited without any addition of random disturbances on temperature or velocity, they may be excited even from very small numerical errors. Here, we seek what kind of disturbances is excited at the initial stage and also how a single mode is selected to grow and others would be faded out. **Fig. 3** and **Fig.4** show snapshots of the velocity vectors and contour lines of temperature deviations on the liquid surface and a horizontal cut plane at Z=0.5 at a very early stages, where the disturbance is defined by substituting an azimuthally averaged instantaneous value, such as;

$$\Theta'_{(R,\theta,Z,f\tilde{N})} = \Theta_{(R,\theta,Z,f\tilde{N})} - \int_0^{2\pi} R\,\Theta_{(R,\theta,Z,f\tilde{N})}\,d\theta \,/\, 2\pi R \qquad (11)$$

and

$$U'_{(R,\theta,Z,f\tilde{N})} = U_{(R,\theta,Z,f\tilde{N})} - \int_0^{2\pi} R\,U_{(R,\theta,Z,f\tilde{N})}\,d\theta \,/\, 2\pi R \qquad (12)$$

As shown in Fig.3, at τ= 0.470 (indicated by **a** in Fig. 2-b), we can see some three-dimensional disturbances, a mixture of m=2 and 3 on Z=0.5 plane, but a structure of m=2 seems prevailing near the liquid surface. But as seen in Fig.4 taken at τ=0.615 (indicated by **b** in Fig.2-b), there is no remaining of m=3 disturbance. This suggests there worked a mode selection rule which determined unique dominant wave number under a given condition. The details of this rule will be discussed later in section 5.5. Once a 3-D disturbance of m=2 is selected, its oscillation amplitude increases exponentially with time for a long time span with a constant value of β. And at around τ=2.7 , a *pulsating*, m=2 oscillatory flow with constant oscillation amplitude was established.

The velocity and temperature distributions of the fully developed *pulsating*, m=2 oscillatory flow at Ma=4440 are exactly the same as those shown in Fig. 12 of Ref.16. Under this condition, *pulsating* type oscillation prevails throughout the time span of the simulation up to τ=4.45.

After the oscillation amplitudes and period settle down to constant values, the Marangoni number was increased instantaneously at τ=4.45 from Ma=4440 to 6660. The transient response was quick and soon a new steady stage of oscillation was established. The velocity and temperature distributions oscillate as a *pulsating*, m=2 type and it sustained pulsating oscillation for long time. **Fig. 5** shows the oscillations of velocity and temperature fields over one period of local azimuthal velocity oscillation (τ_p).

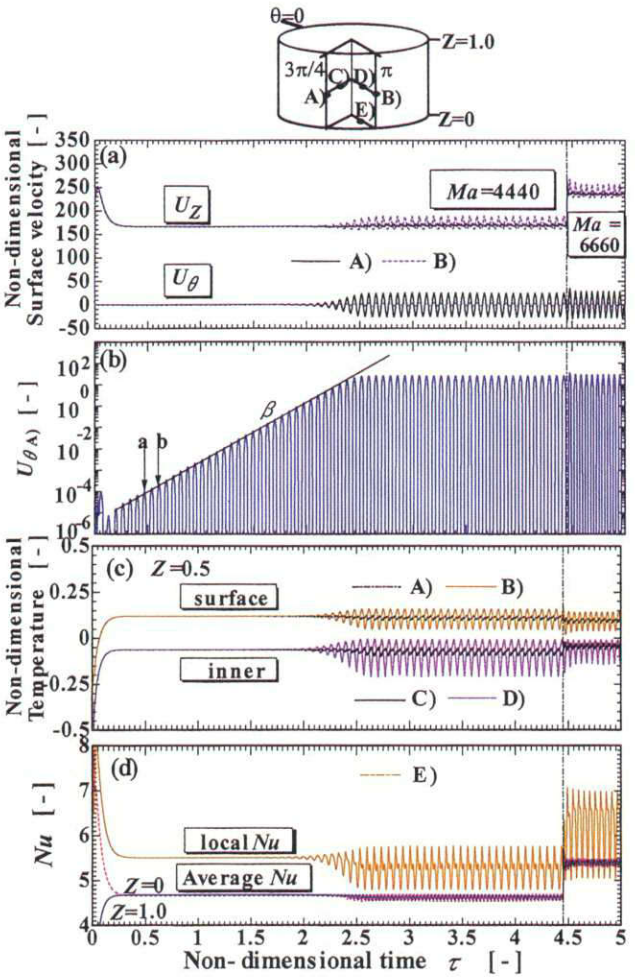

Fig.2 Developments of thermocapillary flow from a quiescent isothermal condition; evolution of velocities, temperatures and Nusselt numbers under *Ma*=4440. At τ= 4.45, *Ma* was raised to 6660.

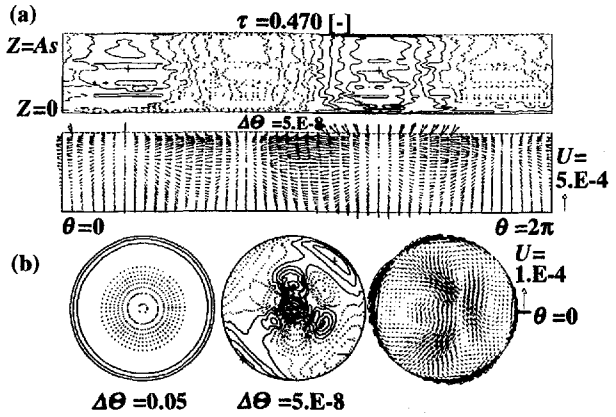

Fig.3 Snapshot of 3-D disturbances at a very early stage of growth, at τ=0.470, under *Ma*=4440.

(a) Contour lines of the temperature disturbance and vector of velocity disturbances on the liquid surface.

(b) Isotherms, contour lines of the temperature disturbance and velocity disturbances on a horizontal cut at Z=0.5. Solid line indicates positive deviation and dotted line indicates negative deviation.

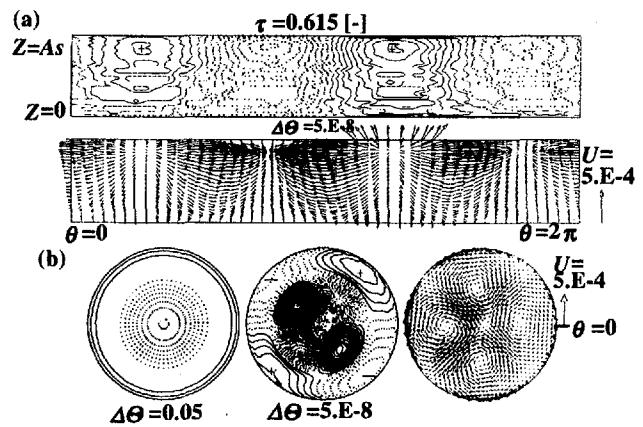

Fig.4 Snapshot of deviation temperature and velocity on the surface and *Z*=0.5 at τ=0.615.

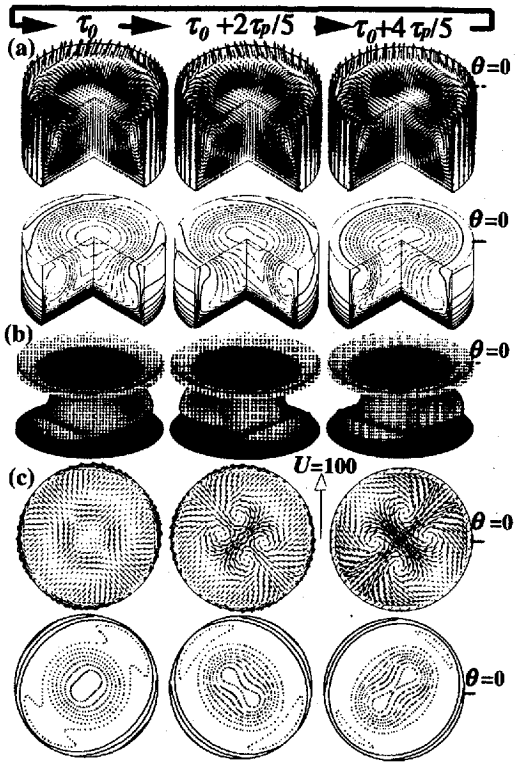

Fig.5 Snapshots over one period of azimuthal velocity oscillation during the fully developed *pulsating* m=2 oscillation under Ma= 6660 after a raise from 4440.

(a) Velocity vectors and isotherms, the upper plane is a horizontal cut at Z=0.85.

(b) 3-D structure of an isothermal surface of Θ= - 0.05.

(c) Projected velocity vectors and isotherms on a cut at Z=0.5.

5.1.2 *Ma*=6660

The second unsteady simulation of self-excitation of oscillatory flow was performed with Ma=6660 and As=1.0. In this case, a 3-D disturbance starts and its mode is selected at a very early stage. Its azimuthal wave number is m=3 and the growth rate is larger than in the previous case of Ma=4440. The oscillation behavior is quite similar to that shown in Fig. 7 in the next section.

5.1.3 *Ma*=8880

The third simulation for As=1.0 was performed with Ma=8880. The time evolution of local velocities, temperatures, and the averaged and local Nusselt numbers are shown in **Fig. 6**. A pulsating 3-D disturbance with m=3 is self-excited and grows much faster than the previous two cases. After the growth period, a fully developed pulsating oscillatory flow with constant amplitude and frequency is established and maintains pulsating oscillation for a while. The velocity and temperature fields vary with time as shown in **Fig.7** during one period of U_θ oscillation (τ_p=0.0349) starting from τ=1.249

(indicated by **a** in Fig.6). As time goes on, a transition occurs from the *pulsating* m=3 oscillation to a *rotating* m=3 oscillation. **Fig.8** compares the power spectrum obtained by means of FFT analyses of local temperature and surface velocities at different points during the *pulsating* and the *rotating* oscillation periods. During the *pulsating* oscillation, some signals show only one fundamental frequency, *i.e.*, $\omega \approx 180$, but $\Theta_{(1.0,0,0.5)}$, $\Theta_{(0.5,0,0.5)}$, $\Theta_{(0.5,\pi/4,0.5)}$, and $U_{z\,(1.0,0,0.5)}$ show second harmonics and the relative strength of the fundamental and the second harmonic varies with the location and, in some cases, the second harmonic appears stronger. In the *rotating* oscillations, however, the second harmonic disappears. This is always the case for all simulation results for Pr=1.0 in this paper. The fundamental frequency of oscillation is practically independent of the type of the oscillation(i.e., *pulsating* or *rotating*). The transition process from the *pulsating* to the *rotating* oscillation is visualized in **Fig.9.** The figure shows temperature and velocity distributions on a horizontal cut at Z=0.5 and on the liquid surface at τ=1.356, 1.570, 1.784 and 1.998 (at points **b, c, d** and **e** in Fig.6, respectively). The transition proceeds with gradual distortions of the temperature and velocity fields near the axis and also on the surface. Kuhlmann and Rath [21] suggested a standing wave type oscillation as a result of the superposition of two hydrothermal waves counter-propagating with angular velocities $\pm\omega$. The *pulsating* oscillation in this fully nonlinear simulation also corresponds to the standing wave type oscillation. During the *pulsating* m=3 oscillations, the flow field consisted of 6 equal sized independent cells. But as time passed, the temperature and velocity fields in the inner region became slightly distorted. Gradually one of the two propagating disturbances ($\pm\omega$) becomes dominant and results in a one-directionally rotating oscillatory flow structure which consists of 3 larger and 3 smaller distorted cells as shown in **Fig.10**. The figure illustrates the temperature and velocity distributions of the rotating m=3 oscillatory flow in almost $0.5\tau_p$ starting from τ=2.50 (at the point **f** in Fig.6). The figure indicates that during a half period of U_θ oscillation, the 3-D structure of m=3 has rotated 1/6 way of its full rotation. If these are observed from a coordinate rotating with a constant angular rotating rate ω, we will see a steadily sustained 3-D structure of temperature and velocity field as shown in **Fig.11**. Therefore the average Nu on both plates converge to a constant value, which is slightly smaller than the averaged Nu value obtained by a 2-D simulation. The local Nu at any point, however, keeps its oscillation.

Fig.12 shows the calculated trajectories of tracer particles over $12\tau_p$, *i.e.*, a time interval that allows 4 rotations of the 3-D structure of temperature-velocity distributions. In spite of the rotation of the 3-D temperature-velocity field, the whole body of the liquid bridge does not follow the rotation. Most of the fluid motions are rather localized. A very small portion of fluid continues long distance azimuthal displacement. But it should be noticed the speed of the azimuthal motion is very small and the particles move rather in the opposite direction to the rotation of the 3-D temperature-velocity field (i.e. propagation direction of the hydrothermal wave).

These three case studies mentioned above indicate that many types of 3-D oscillatory flow will arise depending on the initially imposed Marangoni number (temperature difference between solid discs).

This may explain the reported multi-morphological feature of the 3-D oscillatory Marangoni flows in liquid bridges, *pulsating* and *rotating*, m=2 and 3 (and probably more m's) for As=1.0. At smaller Marangoni numbers, the pulsating oscillation prevails quite a long time. But at larger Marangoni numbers, the *pulsating* oscillation is easily taken over by the *rotating* oscillation.

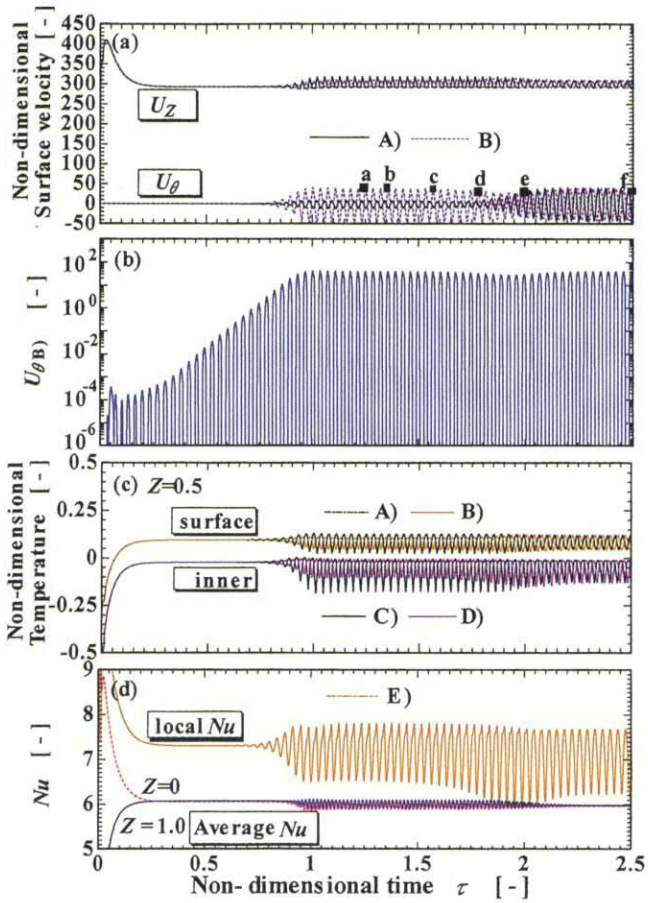

Fig.6 Evolution of 3-D flow under Ma=8880.

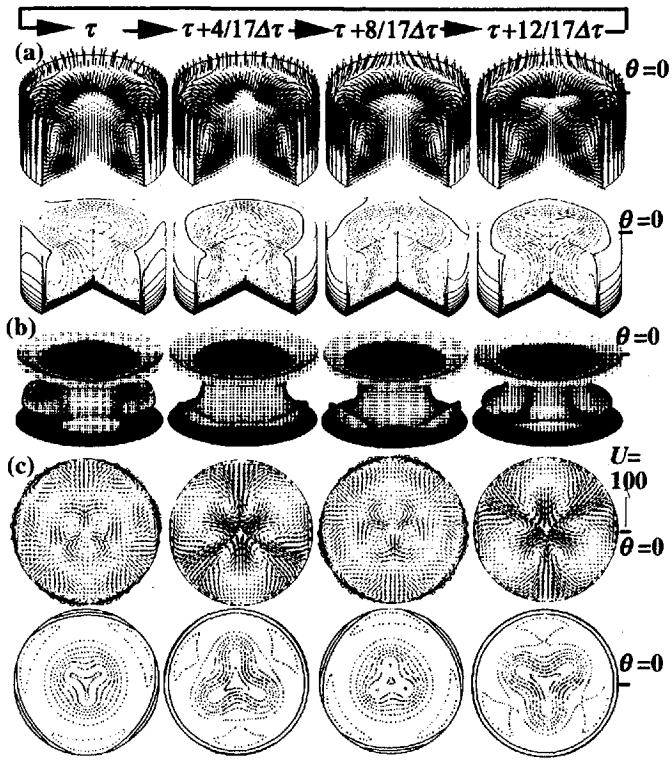

Fig.7 Snapshots of pulsating m=3 oscillation self-excited at Ma=8880 over one period of local velocity oscillation starting from τ= 1.249 indicated by point a in Fig. 6.

(a) Velocity vectors and isotherms, the upper plane is a cut at Z=0.85.

(b) 3-D structure of an isothermal surface of Θ=-0.05.

(c) Isotherms and velocity vectors projected on a cut at Z=0.5.

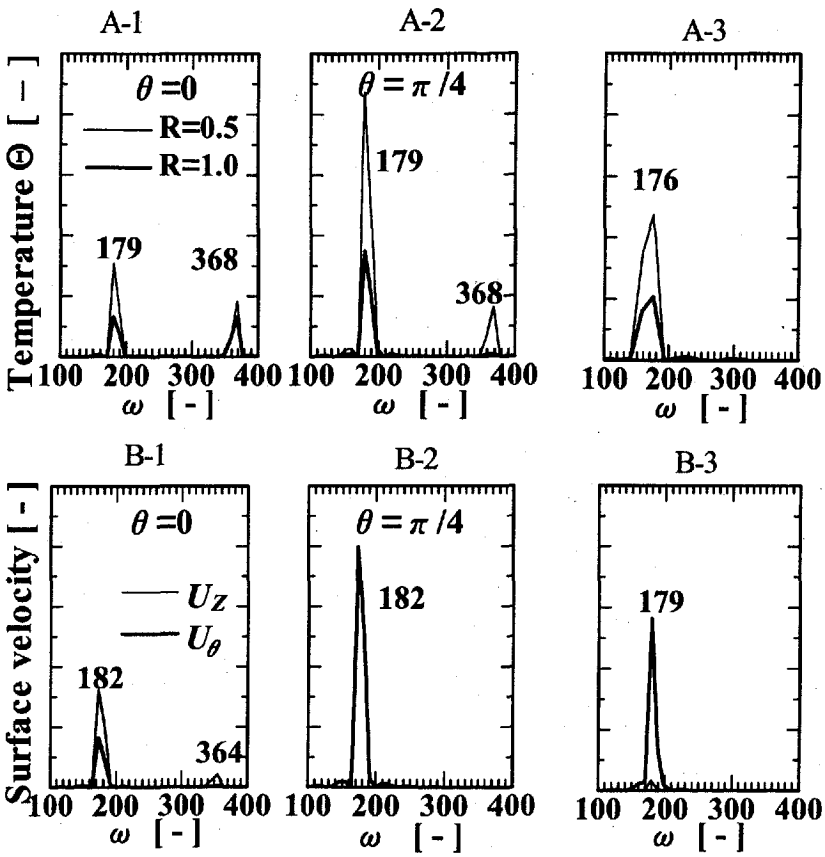

Fig.8 Power spectrum of local temperature and velocity oscillations at *Ma*=8880.

A: Power spectrum of fully developed temperature oscillations at different points. A1 and A-2: during pulsating oscillations, A-3: during rotating oscillations.

A-1 at points (R=1.0, θ=0, Z=0.5) and (R=0.5, θ=0, Z=0.5). A-2 at points (R=1.0, θ=π/4, Z=0.5) and (R=0.5, θ=π/4, Z=0.5). A-3: at point (R=0.5, θ=0, Z=0.5).

B: Power spectrum of fully developed surface velocity oscillations at different points. B-1 and B-2: during pulsating oscillations, B-3: during rotating oscillations.

B-1 U_Z and U_θ at (R=1.0, θ=0, Z=0.5. B-2 U_Z and U_θ at (R=1.0, θ=π/4, Z=0.5). B-3: U_Z and U_θ at any point on Z=0.5 along the liquid surface.

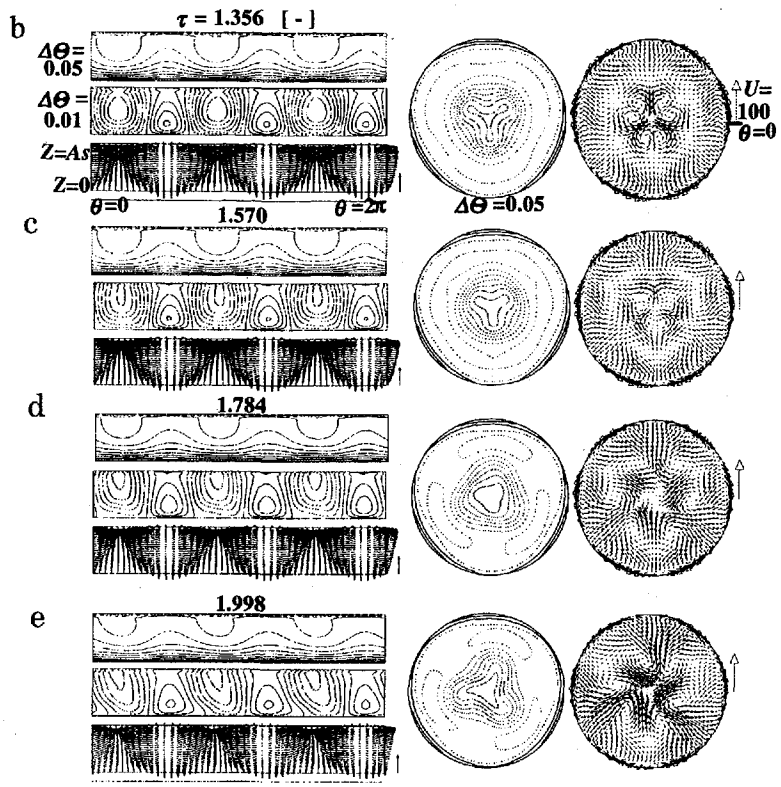

Fig.9 Transition from *pulsating m*=3 oscillation to a *rotating m*=3 under *Ma*=8880. Isotherms, temperature deviation from the 2-D steady solution and velocity vectors on liquid surface and isotherms and velocity vectors on a horizontal cut at *Z*=0.5.

b: at τ=1.356 (at point **b** in Fig.6) , c: at τ=1.570 (at point **c** in Fig.6),

d: at τ=1.784 (at point **d** in Fig.6) and e: at τ=1.998 (at point **e** in Fig.6)

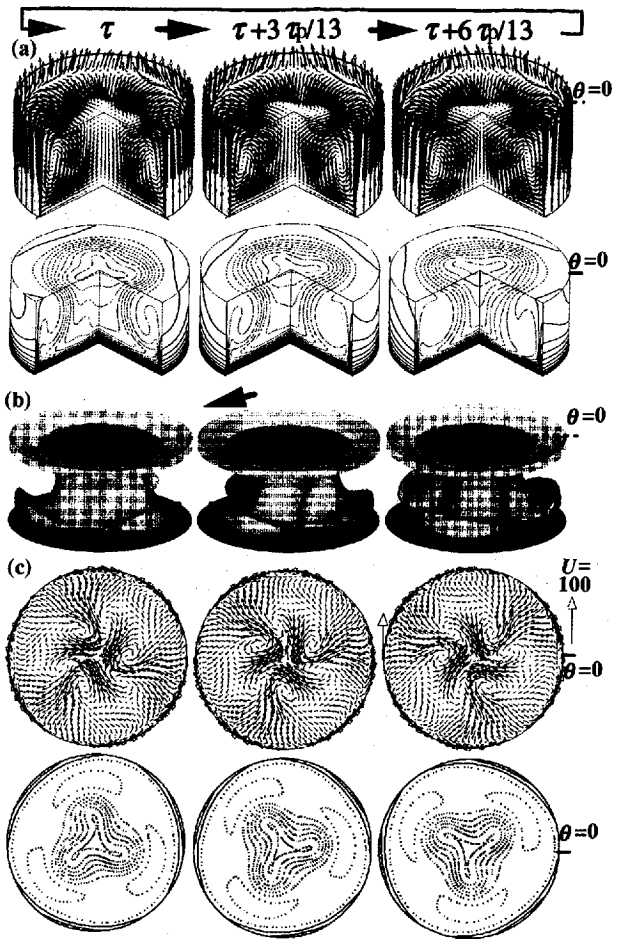

Fig.10 Snapshots over one period of the fully developed *rotating m*=3 oscillation at *Ma*=8880.

(a) Velocity vectors and isotherms, the upper plane is a cut at Z=0.85.

(b) 3-D structure of an isothermal surface of Θ= - 0.05.

(c) Projected velocity vectors and isotherms on a cut at Z=0.5.

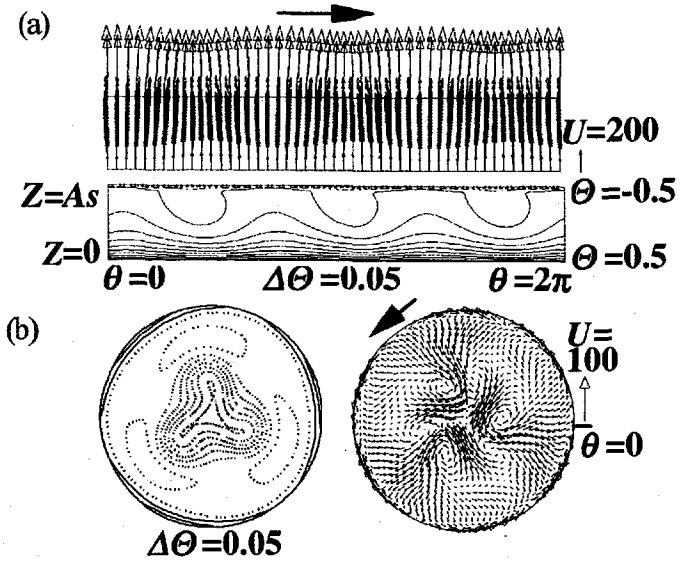

Fig.11 Velocity and temperature distributions during the fully developed *rotating m*=3 oscillation at *Ma*=8880.

(a) Velocity vectors and isotherms on liquid surface. An arrow on the top indicates the rotation direction.

(b) Velocity vectors and isotherms on a horizontal cut at Z=0.5. An arrow indicates the rotation direction.

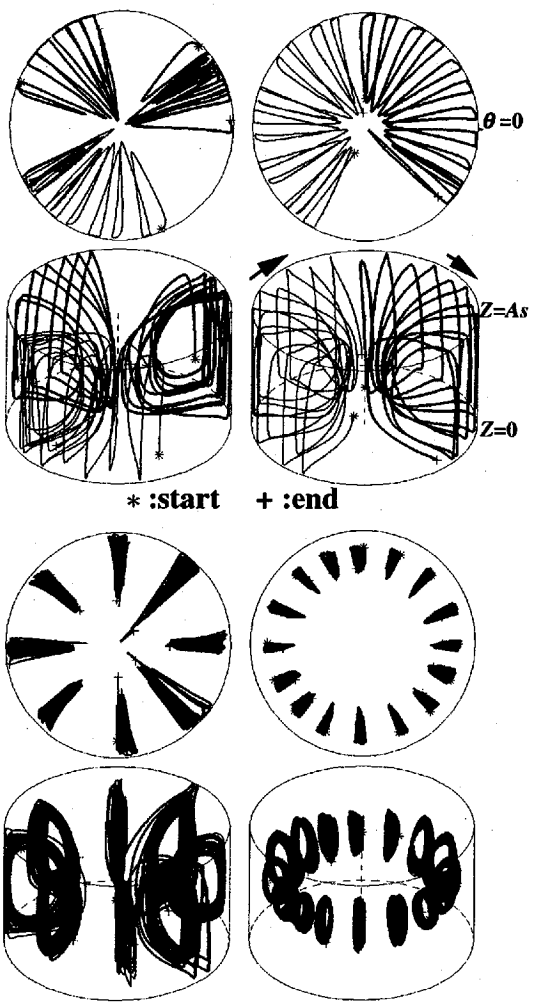

Fig.12 Trajectories of tracer particles during $12\tau_p$ of fully developed *rotating m*=3 oscillation. Top views and birds-eye views.

5.1.4 Growth rate constant and the critical Marangoni number for As=1.0

In order to get information on the growth rate and then to make comparison of the critical Marangoni number with linear stability analysis, transient behaviors under different Marangoni numbers are tested with the 3-D code. Using the final state in Fig.6 as an initial condition, Ma value was decreased instantaneously from 8880 to 2500 and maintained for a short period, then increased stepwise several times. **Fig.13** is the plot of $\ln(U_\theta)$ during these transient calculations. The amplitude of U_θ decreases or increases exponentially with time depending on the Ma value. It should be noticed that the mode of these oscillations was maintained as the *rotating* m=3 throughout the whole range of the Ma change. From these results, the growth rate constant β and the oscillation frequency ω were determined as a function of Ma and shown in **Fig.14**. For a set of data with the same m value, β and ω of the self-excited growing 3-D disturbances (indicated by the key with a horizontal bar) and of those obtained by the procedure illustrated in Fig.13 fall on the same curve. The results indicate that there is a threshold value of Marangoni number at which β is zero and above which an infinitesimal 3-D disturbance starts its growth; *i.e.* the critical Marangoni number Ma_c. The critical Marangoni numbers and the corresponding oscillation frequencies are determined by means of interpolation as: for m=2; Ma_c=2615 ω_c=65.7 and for m=3; Ma_c=3175 ω_c=82.8. The Ma_c for m=2 coincides within 4% of error with the results of the linear stability analysis; Ma_{cL}=2532 and ω_{cL}= 62.1 for m=2 [22]. As linear stability analysis predicts, for liquid bridges of As=1.0 and Pr=1.02, the most dangerous mode of 3-D disturbance is m=2 because it has the smallest value of the critical Marangoni number. The present results of Fig.14 indicate that near this critical value, m=2 mode shows larger β value than m=3 mode. But at larger Marangoni numbers *e.g.* Ma>5600, β value of m=3 exceeds that of m=2. As shown in section 4.2, the 3-D disturbance with m=2 was automatically selected at Ma=4440, and m=3 at Ma=6660 and 8880 during their self-excited growth from the quiescent initial state. These results and Fig.14 suggest that there is a mode selection rule, *i.e.*, the 3-D disturbance which has the largest growth rate constant under a given Marangoni number, is preferentially excited and grows. But if the Marangoni number were changed after an oscillatory flow had been established, the previous oscillation mode sustained itself, as seen in the case of the raise of Ma from 4440 to 6660 in Fig. 3.

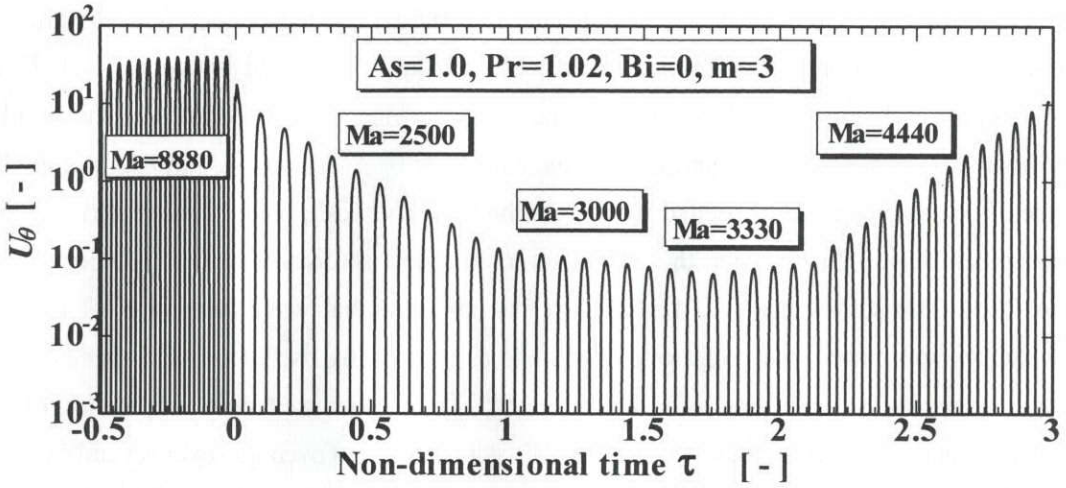

Fig.13 Transient responses of U_θ oscillation to stepwise changes of *Ma*. Starting from the solution at the final state of Fig. 6.

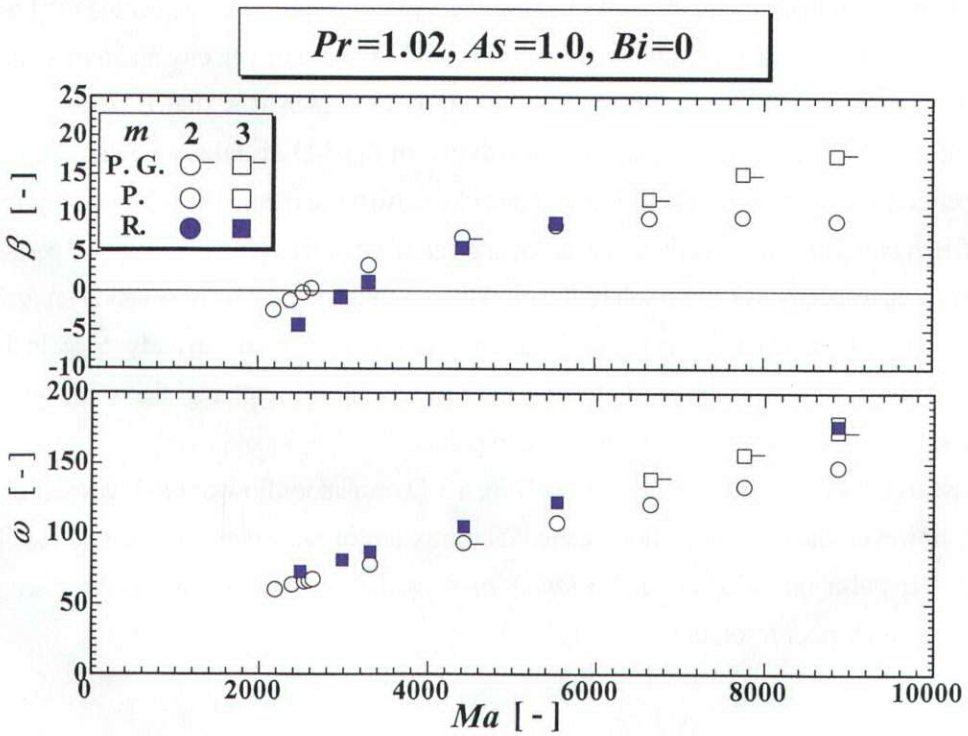

Fig.14 Growth rate constant β and oscillation frequency ω as a function of Marangoni number for *As*=1.0, *Pr*=1.02 and *Bi*=0.

5.2 As=0.75

Fig.15 shows time evolution of the axial and azimuthal velocities at point A(R=1.0, θ=3π/4, Z=0.5As), temperatures at point A and B(R=1.0, θ=π, Z=0.5As) and the average Nusselt numbers at both solid surfaces during a self-excited growth of 3-D flow in a liquid bridge of As=0.75 with Ma=7770 initially being motionless. At the initial transient stage, surface velocity U_z shows a large over shoot due to the step-wise temperature increase at τ=0. As the plot of ln(U_θ) in **Fig.15-(b)** indicates, however, periodic azimuthal motions, although very weak, have been created within the initial transient stage. This indicates the 2-D axisymmetric flow is unstable against 3-D perturbations at Ma=7770. The self-excited 3-D perturbation has an azimuthal wave number m=4 and grew exponentially with time. This oscillatory flow starts as a pulsating oscillation, and maintains itself pulsating over whole time span of calculation (τ=1.9). As the oscillation amplitudes of local temperatures and velocities increase, the average Nusselt numbers (if averaged over several oscillation periods) become slightly smaller than those of the axisymmetric steady flow. **Fig.16** shows some snapshots of the fully developed pulsating m=4 oscillatory flow. Fig.16-a shows the 3-D velocity vectors and isotherms, Fig.16-b; a 3-D isothermal surface at Θ=-0.05, Fig.16-c; velocity and temperature distributions at mid plane (at Z=0.5As), Fig.16-d shows the velocity vectors and isotherms on the liquid surface. The doted isothermal line indicates negative value and the solid line indicates positive value of Θ.

It should be noted that exactly the same 3-D oscillatory flow solution (i.e., *pulsating* m=4 oscillatory flow with the same oscillation amplitudes, frequency and structure of velocity and temperature fields as shown in Figs.15 and 16 was obtained by a simulation which was started from a 2-D steady solution at Ma=7770. And in this case, the growth rate of the 3-D disturbance with m=2 during the growth period (i.e., the slope of the ln(U_θ) vs. t plot) was also the same as that shown in Fig.15-b.

In Ref.16 a *pulsating*, m=3 oscillation was obtained at Ma=5920 (with 34, 57, 32 grid points in R, θ, and Z direction, respectively) as a result of the growth rate enhancement by postulating an azimuthally asymmetric (m=3) heat exchange between the ambient gas for a short time in early stage. In this work, similar *pulsating*, m=3 oscillatory flow was also incubated by applying the same growth rate enhancement under Ma=7770 with 45, 65, 40 grid points.

If we use a coarser grid (34, 57, 32) at Ma=7770, a 3-D oscillatory flow of m=4 was self-excited. In this case, however, the oscillatory flow started as a mixture of *pulsating* and *rotating* oscillation of m=4 and later pulsation faded out and *rotating*, m=4 oscillatory flow remained. We discarded this result because of its poor resolution.

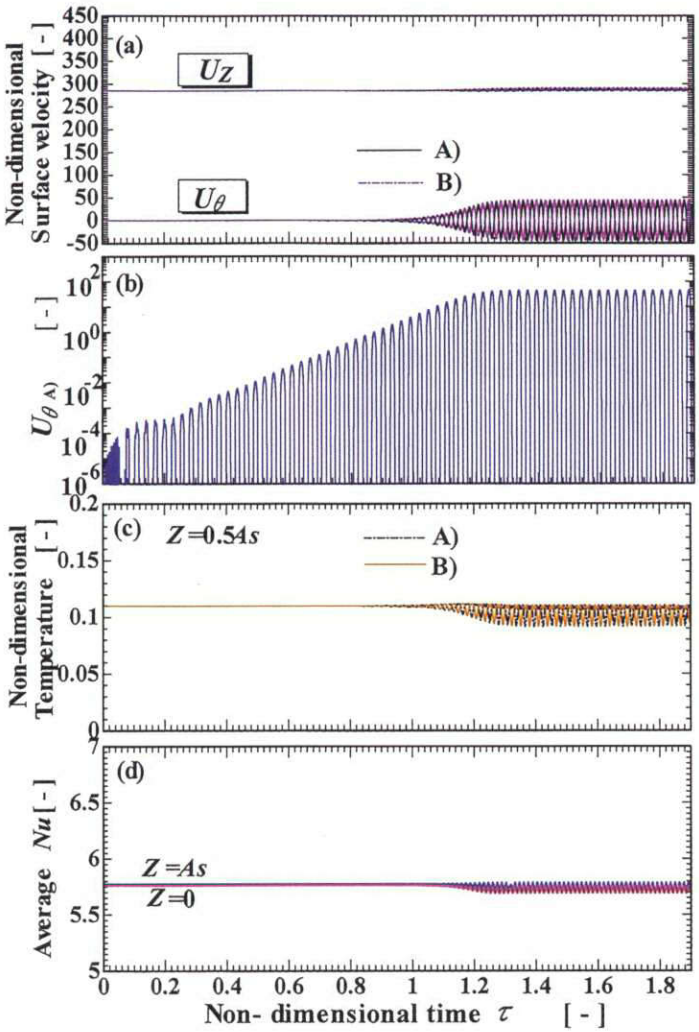

Fig.15 Time evolution of self-excited 3-D oscillatory Marangoni flow in As=0.75, Ma=7770 and Bi=0. Mode of the fully grown 3-d flow is m=4.

(a) $U_z$and U_θ (b) ln(U_θ), (c) Θ, (d) average Nusselt number at both solid disks.

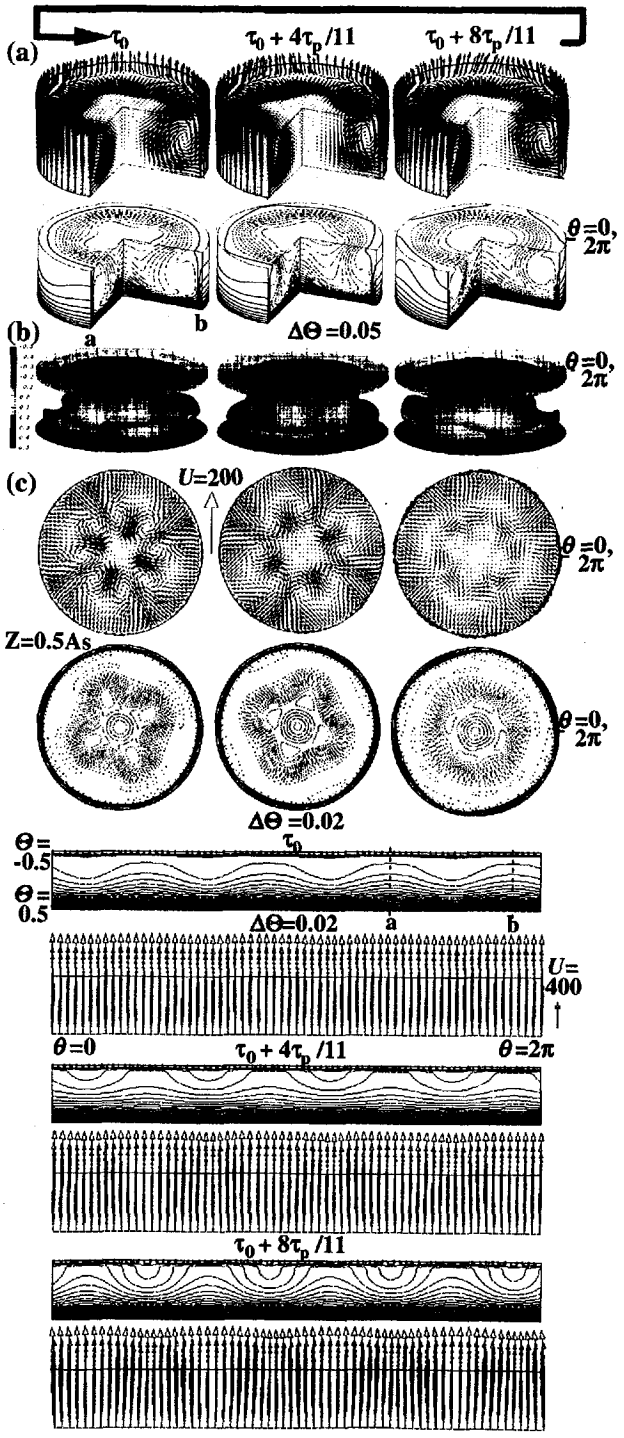

Fig.16 A series of snap-shots of velocity vectors and temperature distributions

(a), 3-D isothermal surface (b), velocity and temperature distributions on a horizontal cut at Z=0.5As (c) and isotherms and velocity vectors on the surface (d), over one period of the fully developed *pulsating* m=4 oscillation under Ma =7770 and As=0.75.

5.3 As=1.33

Fig. 17 shows time evolution of azimuthal velocity at point A(R=1.0, θ=π/2, Z=0.5As), axial and azimuthal velocities at point A and B(R=1.0, θ=3π/4, Z=0.5As), local temperatures, local and spatially averaged Nusselt numbers at Ma=3330. In this case, a pulsating type oscillation with m=2 was self-excited and reached a constant amplitude pulsating oscillation stage. **Fig. 18** shows instantaneous velocity and temperature distributions at the mid-plane (at Z=0.5As) and temperature and velocity distributions on the surface, during one period of oscillation at fully developed stage. The cold plume, which would have flown down coaxially along the axis if the flow is axisymmetric, sprits into two and flow down asymmetrically. On every half period, the axes of the cold plumes shift azimuthally by π/2 almost instantaneously. The liquid bridge is separated into four equal sized cells. This pulsating oscillation corresponds to the standing wave composed by the two equivalent hydro-thermal waves propagating in opposite azimuthal directions[21].

But around τ=2.5, the temperature oscillations in inner part (at points c and d) exhibited some phase sift and the transition to a rotating oscillation starts. The transition proceeded in a way similar to that reported for m=3 oscillatory flow in a liquid bridge of As=1.0 [22]. Finally the pulsation faded out and a rotating oscillation established its steady oscillation by τ=3.6. The rotating oscillation corresponds to a traveling hydro-thermal wave. **Fig. 19-a** shows a snapshot of the rotating m=2 oscillation. The detailed explanations of the rotating m=2 flow was described in Ref.16. During one period of a local temperature oscillation, the combined 3-D structure of temperature and velocity fields (hereafter it is called 3-D structure) rotates 1/2 (=1/m) way of its full rotation. In order to clarify the fluid motion during the rotating oscillatory flow, tracer particles were released at τ=4.19. The isothermal plane at this instance is also shown in Fig.19-b. Some of their trajectories during 7.5 periods of local temperature oscillations (i.e., during 3.75 rotations of the 3-D structure) are plotted in Fig.19-c. As was pointed out for a 3-D flow [22] with m=3, the movability of fluid element is strongly dependent on its initial position. The fluid element near the surface tends to show slow but long distance azimuthal migration in opposite direction against the propagation of the hydro-thermal wave. On the other hand, the inner fluid elements remain within rather confined zone, regardless the unidirectional rotation of the 3-D structure.

Another simulation was conducted with Ma=6660 and As=1.33. A 3-D oscillatory flow of m=2 was also self excited, grew and reached to a constant amplitude pulsating oscillation and then a transition occurred to rotating m=2 oscillation. The resultant rotating m=2 oscillatory flow was exactly the same as that reported in Ref.16.

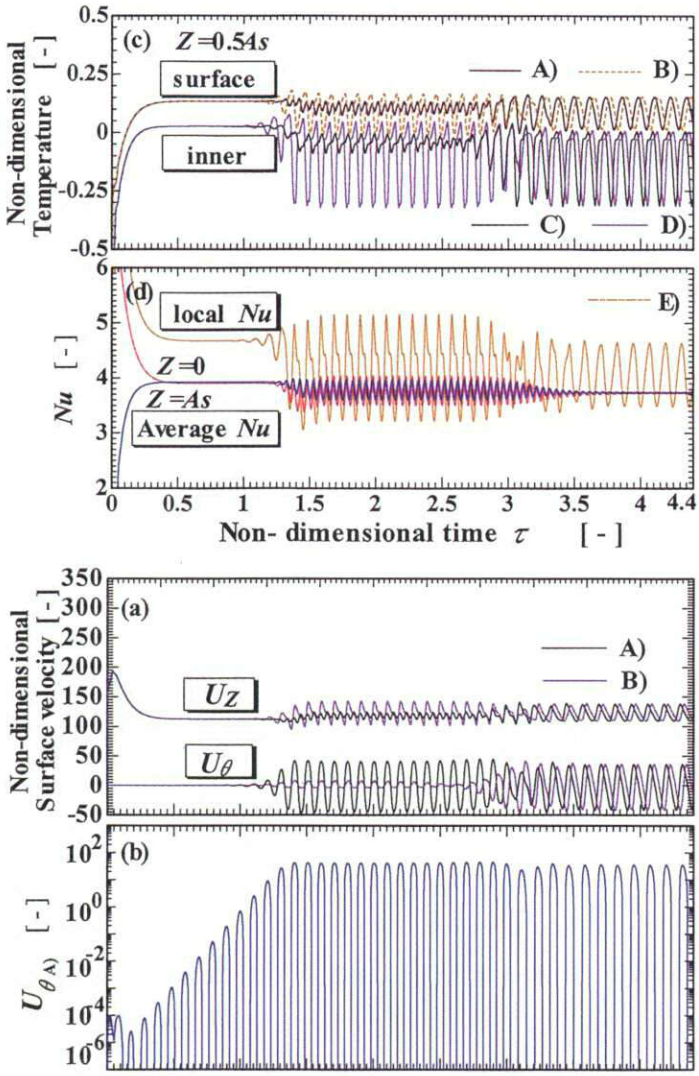

Fig. 17 Time evolution of self-excited 3-D oscillatory Marangoni flow in *As*=1.33, *Ma*=3330 and *Bi*=0. Mode of the fully grown 3-d flow is *m*=2.

(a) U_z and U_θ, (b) ln(U_θ), (c) Θ, (d) local and average Nusselt numbers at both solid disks.

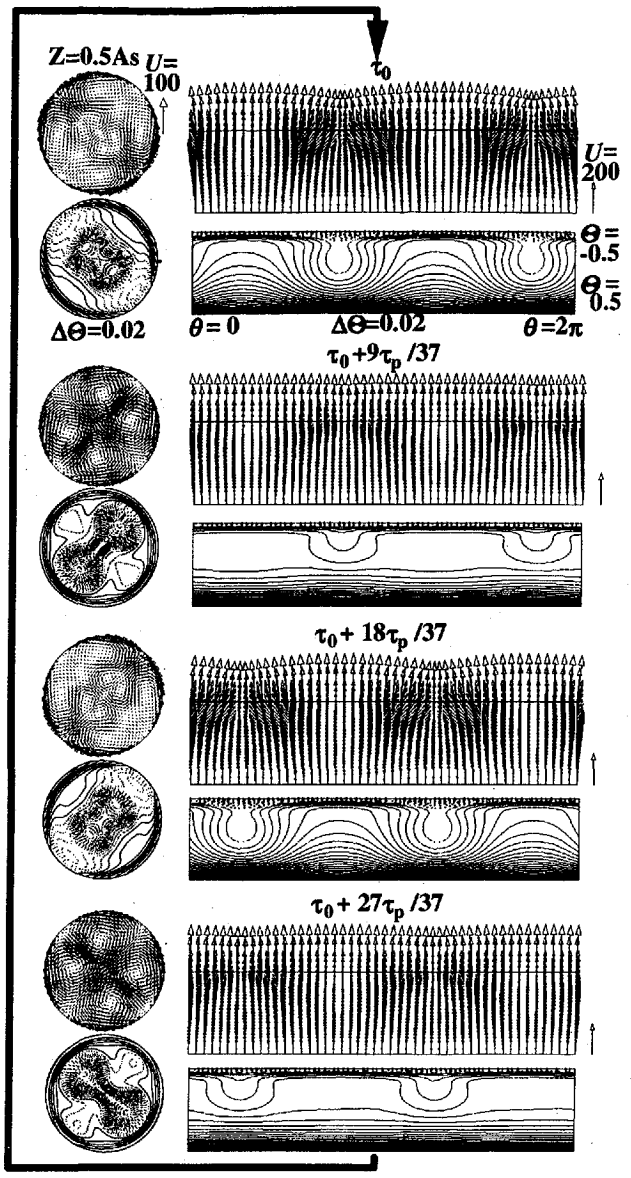

Fig. 18 Snapshots over one period of *pulsating m*=2 oscillations under *Ma*=3330, *As*=1.33; velocity vectors and isotherms on the surface and mid plane (at *Z*=0.5*As*)

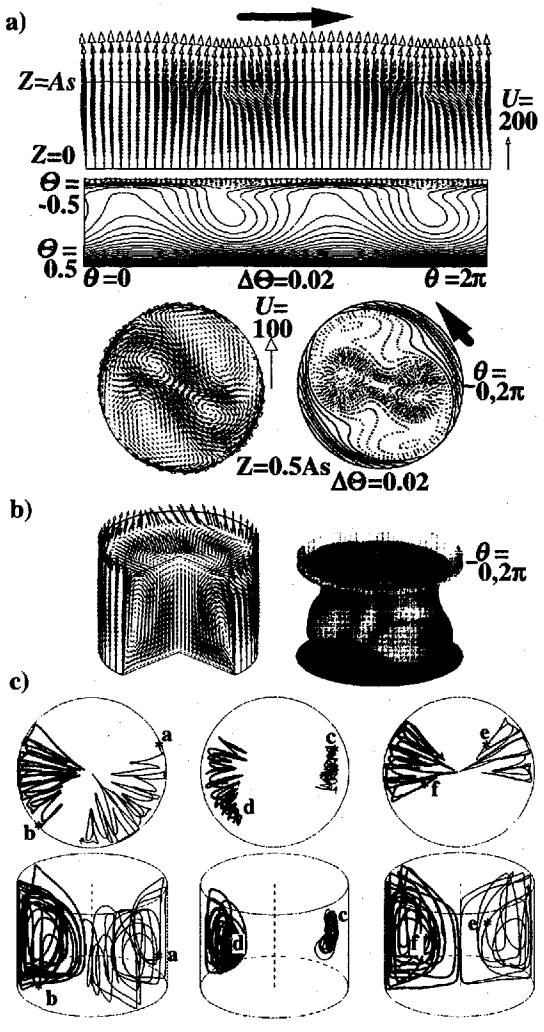

Fig. 19 Characteristics of a fully developed *rotating m*=2 oscillation under *Ma*= 3330, *As*=1.33.

(a) velocity vectors and isotherms on the surface and mid plane (Z=0.5As), 3-D isothermal surface at τ=4.19.

(b) trajectories of tracer particles released at τ=4.19 and the points indicated by * and reached to the point indicated by + during 7.5 periods of local temperature oscillations.

5.4 As=1.60

Fig. 20 shows the time evolution of a 3-D oscillation in a slightly longer liquid bridge with As=1.60 under Ma=2220. The self-excited and fully developed 3-D disturbance in this case has a structures of m=1. But for rather long time during growth (up to τ=1.7), pulsating 3-D disturbances with m=1 and 2 seemed to compete each other. Finally, disturbance with m=1 became dominant. A pulsating oscillation prevails in the initial stage (τ<3.9). In this *pulsating* m=1 oscillation, a cold plume flows down off-center, and the axis of the cold plume swings back and forth on every half period along a straight path as shown in Fig.4 of Ref.16. The pulsating oscillation under this Marangoni number lasted longer than the case reported in Ref.16, however, a transition to the rotational mode started at τ=3.9 accompanied with phase shifts in local temperatures and velocities. When the rotating oscillation is fully developed (τ>4.7), the averaged Nu converges to a constant value (Nu=3.05) slightly smaller than that of steady axisymmetric flow (Nu=3.21), although the local Nu keeps periodic oscillation. Some snapshots of the fully developed rotating m=1 oscillation are shown in **Fig. 21**. Trajectories of tracer particles during 4 periods of the temperature oscillation (or during 4 rotations of the 3-D structure) are shown in **Fig. 22.** Fluid elements move over much wider area than the case of As=1.33 (Fig.19-c). Some fluid elements flow across the axis, justifying the experimental observations of tracer motion in m=1 oscillatory flow [1]. It should be noted again that fluid elements migrate in opposite direction to the hydro-thermal wave's propagation.

The velocity vector in Fig. 21 shows two vortices on the middle plane (at Z=0.5As). Similar vortex-pair was observed by Ar et. al.[23] by means of a PIV technique in m=1 oscillatory Marangoni flow in a liquid bridge of silicon oil (Pr=105.6) with highly distorted surface (see Fig.9 of Ref.23).

As shown in **Figs.23** and **24**, the self-excited 3-D flow under Ma=4440 grew up as a *pulsating* m=2 oscillation and there seemed no indication of transition to a *rotating* m=2 oscillation within the calculated time span (τ<3.4). This is the only case of pulsating oscillation being preferred to the rotating one at larger Marangoni number.

By being started from a 2-D steady solution for Ma=4440, our 3-D simulation code also gave an m=2 pulsating oscillating flow. As shown in **Fig. 25**, the incubation process in this case is quite different from that of Fig. 23. However, the structures and characteristics of the finally attained constant amplitude oscillatory flow were exactly the same as those self excited from quiescent isothermal liquid.

This result again confirms the uniqueness of the oscillatory flow solution under a given Marangoni number.

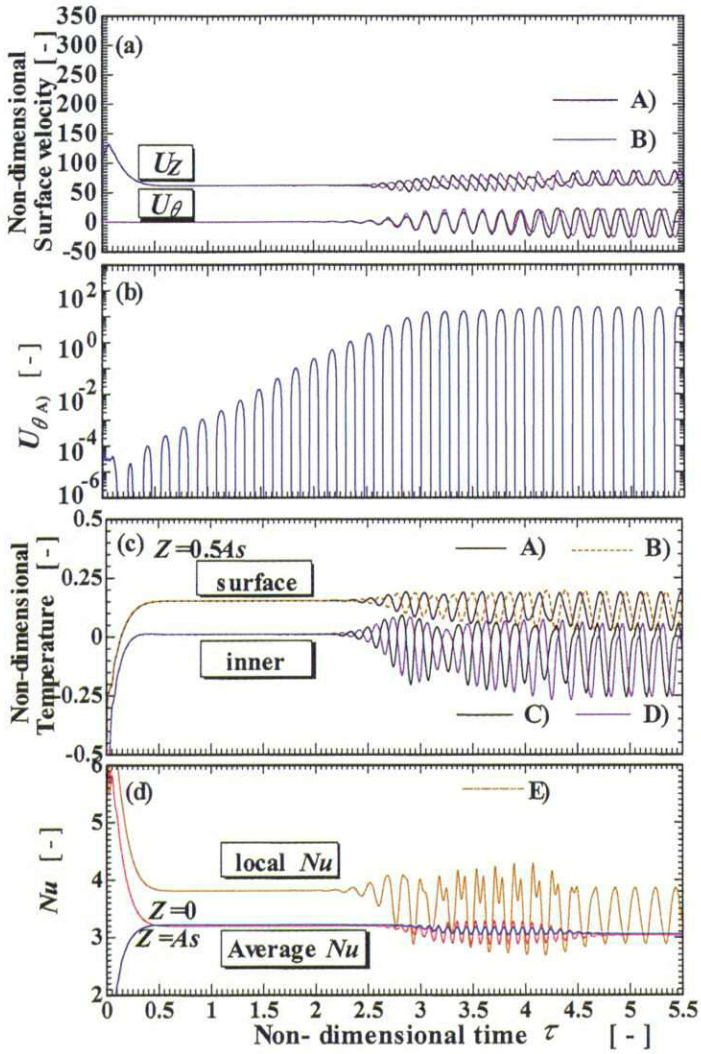

Fig.20 Time evolution of 3-D flow under *As*=1.6, *Ma*=2220. A *pulsating m*=1 oscillation is first developed and then exhibited a transition to *rotating m*=1 oscillation.

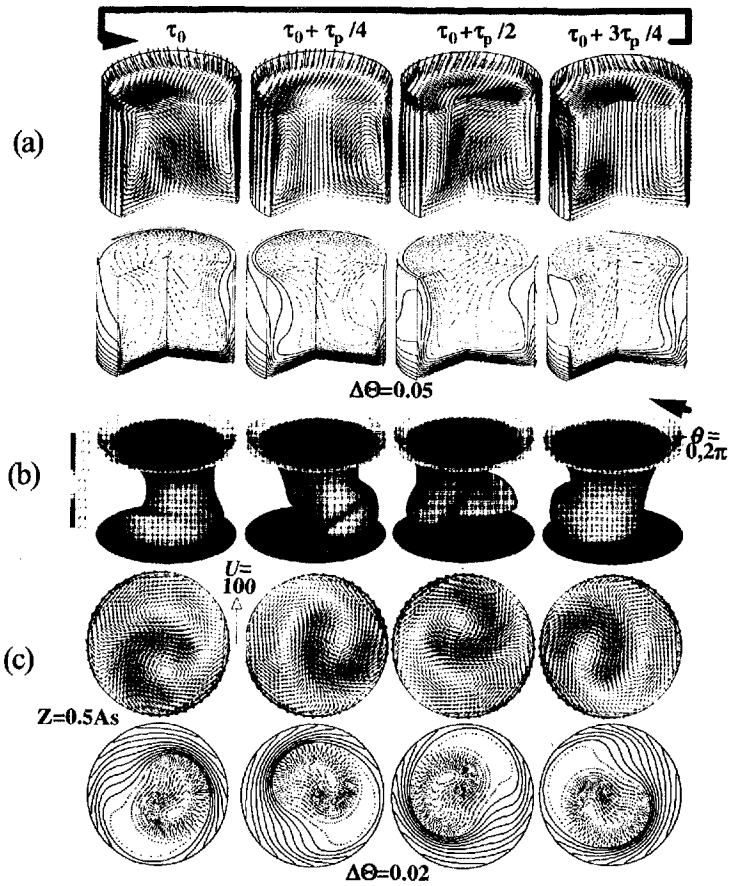

Fig.21 Snap-shots over one period of rotating m=1 oscillation, self-excited at Ma=2220, As=1.6.

(a) Velocity vectors and isotherms, the upper plane is a cut at Z=0.85As.

(b) 3-D structure of an isothermal surface of Θ=-0.05.

(c) projected velocity vectors and isotherms on a cut at Z=0.5As.

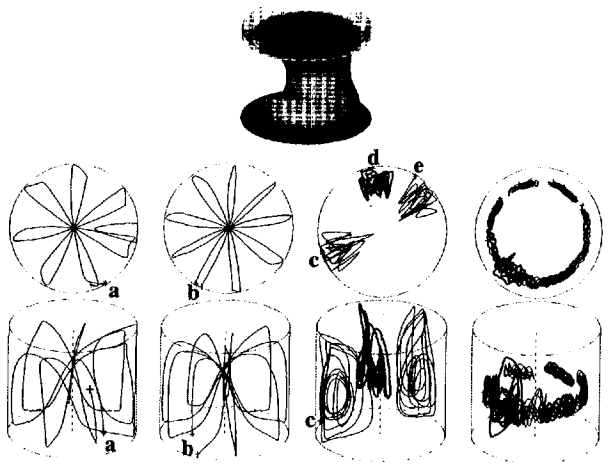

Fig.22 Trajectories of tracer particles released at τ=5.265 and the points indicated by * and reached to the point indicated by + during 4 periods of local temperature oscillations in fully developed rotating oscillatory flow under Ma=2220 and As=1.6.

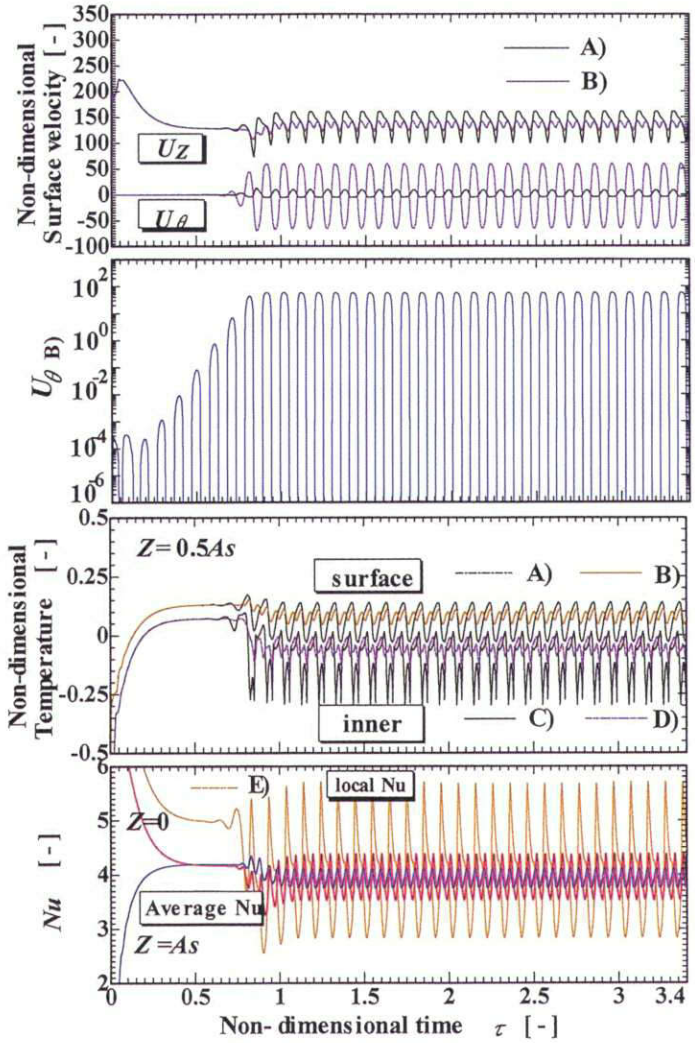

Fig.23 Time evolution of 3-D flow under *As*=1.60, *Ma*=4440. A *pulsating m*=2 structure was self-excited from a quiescent liquid bridge.

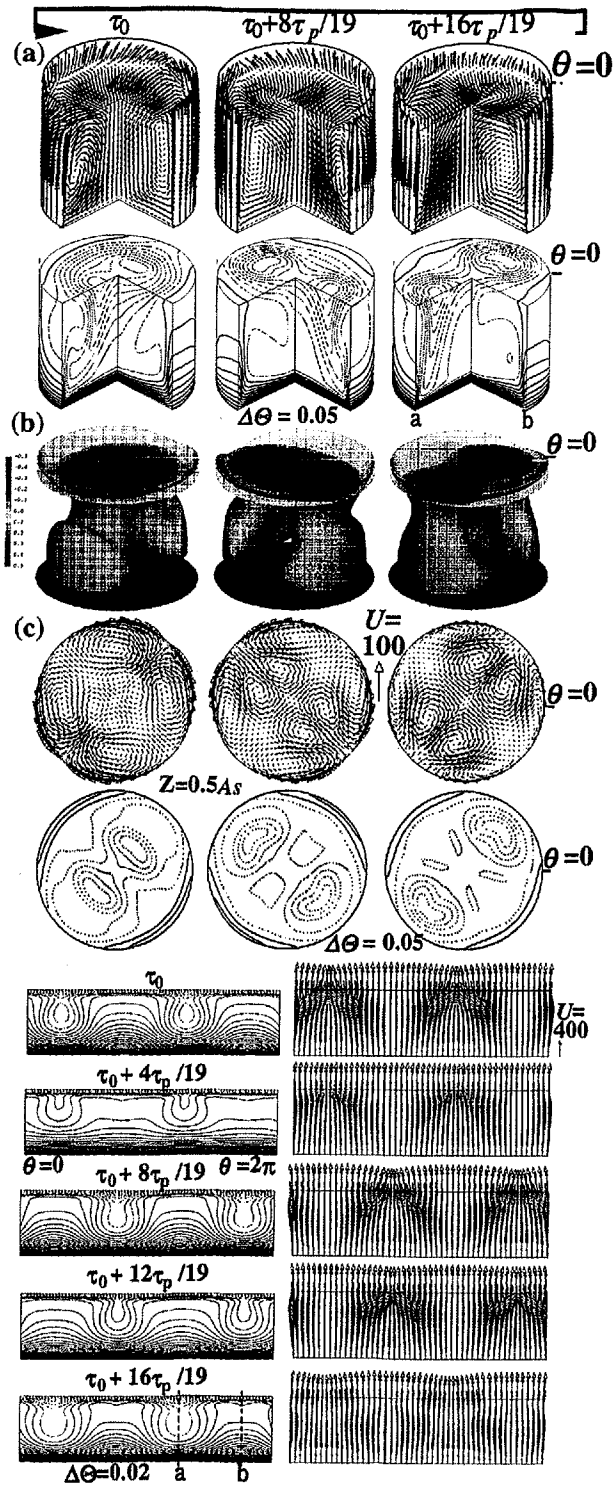

Fig.24 Snap-shots of the fully developed *pulstating m*=2 oscillation at *Ma*=4440 and *As*=1.60.

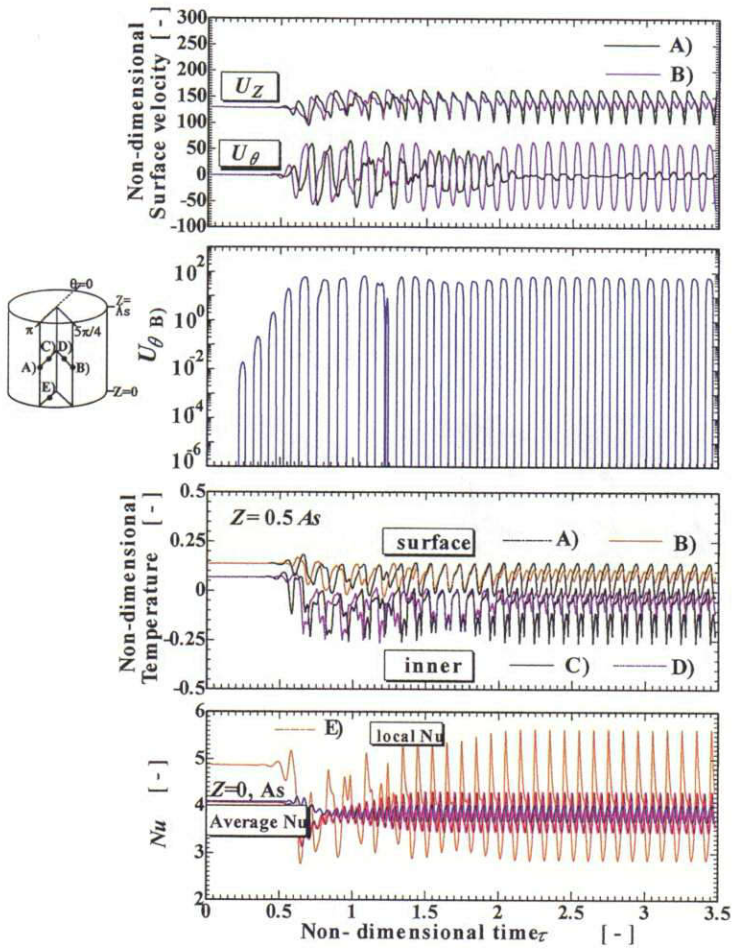

Fig.25 Time evolution of 3-D flow under *As*=1.60, *Ma*=4440. A *pulsating m*=2 structure was self-excited from 2-D steady axisymmetric flow.

5.5 Growth rate of the 3-D disturbances

The 3-D numerical code is used to clarify the transient response of the oscillatory flow to stepwise decreases or increases of Marangoni number, as was illustrated in **5.1.4**. During these processes, the type (*pulsating* or *rotating*) of the oscillation was maintained its initial type, i.e., that of the fully developed oscillation. We have never experienced any transition from *rotating* to *pulsating* or vice versa and shift of azimuthal wave number, m, caused by the serial change of Ma in the present series of simulations for wide range of m, Ma and As.

The logarithmic plot of U_θ indicates that the growth of the oscillatory flow are well approximated by an exponential function over very wide range of amplitude, and the slope of the line segment connecting the peaks in $\ln(U_\theta)$ vs. τ plot provides β value. Thus determined β values and frequencies ω are plotted in **Fig. 26** as a function of Ma for all As and m studied here. From these plots for each condition, we can determine the critical Marangoni numbers Ma_c, at which β becomes zero, above which the disturbances grow ($\beta>0$) and below which they decay ($\beta<0$). Thus obtained Ma_c and critical oscillation frequency ω_c are tabulated in **Table 1**. These fall very close to the corresponding values predicted by the linear stability analysis, the deviations are mostly within 4%, but discrepancy as large as 8% was observed for As=0.75. From our simulations for As=0.75, the most dangerous mode is m=4, i.e., the Ma_c of m=4 is smaller than that of m=3. This is controversial to the result of a linear stability analysis which predicts m=3 mode as the most dangerous mode. This discrepancy may be attributed to the insufficient axial and azimuthal grid points in the present numerical simulations.

Beside the critical Marangoni numbers, the present simulations reveal the order of magnitude of the growth rate constant β and oscillation frequency ω over wide range of the Marangoni number.

In **5.1.4**, we proposed a mode selection rule: i.e., a 3-D disturbance, which possesses largest growth rate constant under a given condition, can grow up selectively. All case studies in this report satisfied this mode selection rule. This fact indicates the validity of our mode selection rule.

Table 1 Critical Marangoni numbers and frequencies.

As	m	Present results		Linear stability theory	
		Ma_c	ω_c	Ma_{cL}	ω_{cL}
0.75	3	5424	144.2	4944	129.2
	4	5350	161.3	5775	166.7
1.00	2	2615	65.7	2532	62.1
	3	3175	82.8	-	-
1.33	2	1772	42.0	1752	41.1
1.60	1	1430	28.3	1413	27. 4
	2	1781	36.5	1734	35.5

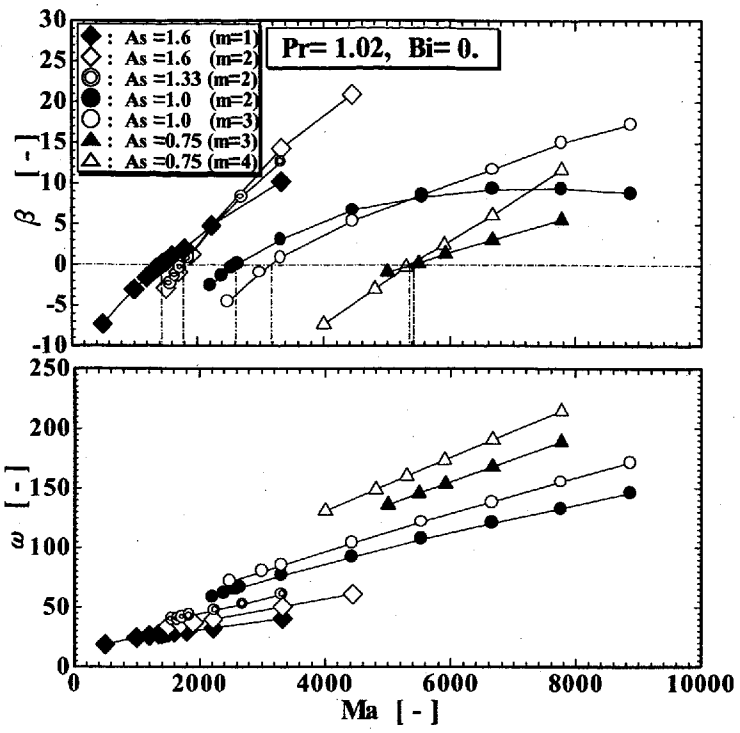

Fig.26 Growth rate constant β and oscillation frequency ω at different aspect ratios and Marangoni numbers for all calculated results.

5.6 Experimental Observability

Many experiments have been conducted to determine critical Marangoni number under microgravity and normal gravity. In these experiments, the incipience of the oscillatory flow has been detected by the observation of oscillation of temperature or velocity. As has been reported by Carotenuto et al.[24], the oscillation amplitude grows very quickly after the first small amplitude oscillation was detected. The present numerical simulations indicate that there must be an incubation period during which 3-D disturbance is growing but is not yet observable. As Ma approaches to Ma_c, the growth rate constant approaches to zero and then the incubation time becomes infinitely long. Therefore, the experimental determination of the true critical Marangoni number seems very difficult.

In order to obtain some idea on the observability of 3-D oscillatory convection, the results in Fig.26 were re-plotted in **Fig. 27** as a function of $(Ma/Ma_c - 1)$. The figure suggests a very crude correlation for β as follows,

$$\beta = B\left\{\frac{Ma}{Ma_c} - 1\right\}^n \qquad (13)$$

The least square method was applied for the whole set of data in Fig.26, which includes the results of As=1.0 [22], to give B=10.7 and n=0.89. It should be noted that this equation is too crude to calculate precise value of growth rate constant and should be avoided for such purpose as the mode prediction.

Equation (13) suggests the following discussion on the experimental observability of the incipience of the 3-D oscillatory Marangoni flow in half-zone liquid bridges.

An experiment is always subjected to imperfections such as surface roughness, geometrical asymmetries, thermal asymmetries, thermal fluctuations, etc. These imperfections are always present at some noise level even at sub-critical conditions. The spectral decomposition of these noises will contain a certain small but finite amplitude (ψ_0) of the critical mode. When the Marangoni number is

$$\psi = \psi_0 e^{\beta\tau} = \psi_0 e^{B(Ma/Ma_c - 1)^n t\alpha/a^2} \qquad (14)$$

increased beyond its critical value, the critical mode with amplitude ψ_0 will grow exponentially with time, independent of other modes. We assume that the growth will continue in the form where we used Eq.(13) for β. The experimental instrument will detect the perturbation only if a certain threshold amplitude ψ^* well above the noise-level is exceeded. That means the apparent critical conditions correspond to

$$\psi^* = \psi_0 e^{B(Ma_a/Ma_c - 1)^n t\alpha/a^2} \qquad (15)$$

where Ma_a is the apparent critical Marangoni number. If now the observation time is limited to a constant value t_0, The apparent critical Marangoni number will be

$$\left(\frac{Ma_a}{Ma_c} - 1\right)^n = \frac{\ln(\psi^*/\psi_0)\, a^2}{\alpha B t} \qquad (16)$$

or

$$Ma_a = Ma_c\left[1 + \left(\frac{\ln(\psi^*/\psi_0)}{\alpha B t_0}\right)^{1/n} a^{2/n}\right] \qquad (17)$$

Therefore the deviation of the apparent critical Marangoni number from the true critical Marangoni number will scale with the radius of the liquid bridge, such as $a^{2/n} \approx a^2$, provided the observation period t_0 is kept constant. Let us assume Eq.13 and Eq.14 hold over wide range of Ma/Ma_c with B=10.7 and n=0.89, and the fluid KCl (α=7.2x10^{-7} m^2/s). Eq.17 predicts a size dependency of the apparent critical Marangoni number as shown in **Fig.28** for different values of t_0 and (ψ^*/ψ_0). The results indicate the observation period t_0 is the most important factor and the value of (ψ^*/ψ_0) gives a minor effect. It should be noted that an extremely long observation time is required to detect the true critical Marangoni number using large liquid bridges.

As shown in Fig.28, Eq.(17) predicts $Ma_a \approx a^2$ at large radius. This explains qualitatively the experimentally determined size dependency of the apparent critical Marangoni number, i.e., roughly $Ma_a \approx a^{1.5}$, as reported by Masud et al.[25] and Carotenuto et al.[24] .However, the following points made quantitative discussions difficult. It is not known whether the observation period t_0 has been kept constant for the measurements of Masud et al.[25], and how much time they allowed. In the experiments of Carotenuto et al.[24], temperature boundary condition was different from this numerical simulation since they used non-steady ramped temperature difference method.

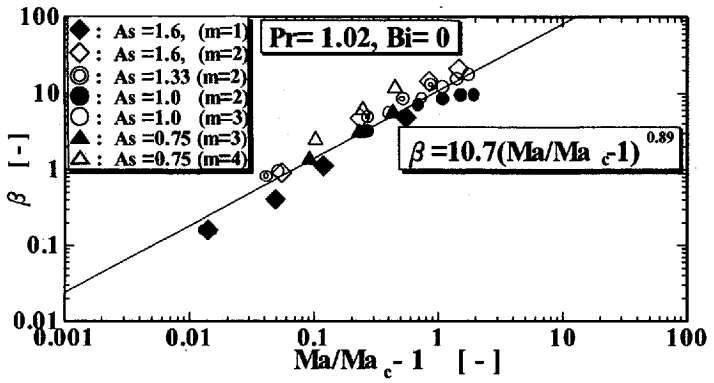

Fig.27 Logarithmic plots of β and (ω/ω_c) vs. $(Ma/Ma_c\text{-}1)$.

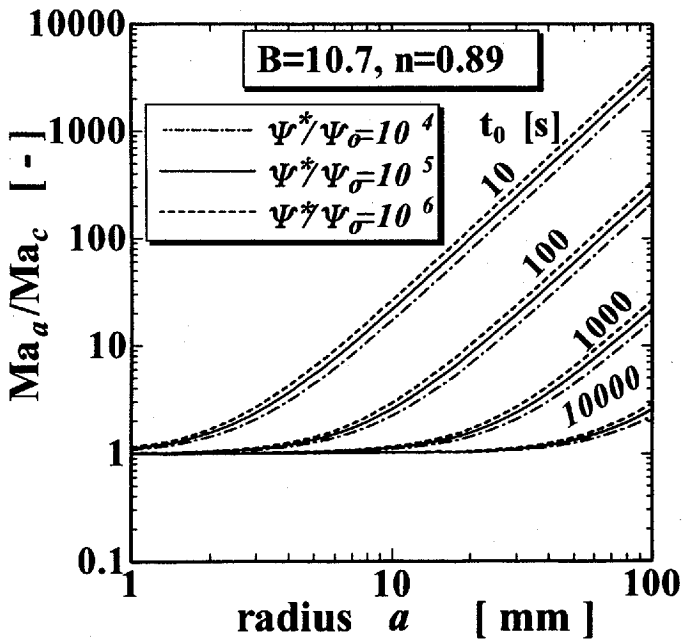

Fig.28 Bridge size dependency of the apparent critical Marangoni number predicted by Eq.17 drawn for molten KCl liquid bridges.

5.7 Effect of an external perturbation on growth rate of 3-D disturbance

In this section, we will show that the growth rate of the 3-D disturbance can be enhanced by some external perturbations such as vibrations, non-uniform heat exchange, *etc.* The next simulation illustrates the effect of a temporary non-uniform heat exchange between ambient gas by assuming an azimuthally non-uniform heat transfer coefficient (Bi=0.025sin2θ) with the ambient gas at T_m=(T_c+T_h)/2 for a short time duration. This trick was adopted in our previous papers [15,16] in order to shorten the incubation time of the 3-D disturbance at a highly super critical condition. **Fig. 29** compares the time evolution of U_θ with and without the temporary non-uniform heat exchange. The temporal heat exchange condition was applied only for the time interval indicated in Fig.29. The non-uniform heat exchange provids a stepwise increase of amplitude by a factor of as much as 10^3 or more within a 1.5 period of oscillation. Despite the enhanced growth rate and a small phase shift of oscillation, the established fully 3-D oscillatory flow has exactly the same structure as the self-excited 3-D flow under Ma=4440.

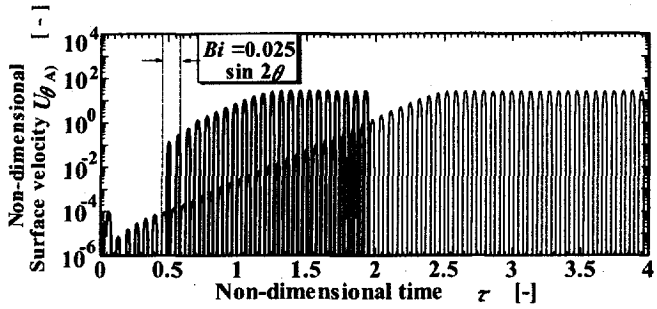

Fig.29 Effect of the external disturbance on the growth of 3-D flow under Ma=4440.
Comparison of the time evolution of U_θ with and without an azimuthally non-uniform heat exchange with the ambient gas (Θ=0) via Bi=0.025sin2θ for a short duration indicated in the figure.

6. Results with low Prandtl number fluids

In the previous sections, we described the oscillatory Marangoni convections in a rather high Prandtl number fluid (Pr=1) . In these cases, the axisymmetric steady flow becomes unstable to three dimensional disturbances at certain Marangoni number and the three dimensional flow always start as either a pulsating oscillation or a rotating oscillation. In the case of low Prandtl fluid's half-zone, the transition takes from an axisymmetric to a steady three dimensional flow at a first critical condition. The steady three dimensional flow becomes unstable and a second transition to a three dimensional oscillatory flow takes place at higher temperature difference. The first critical number is predicted by linear stability analyses. Linear stability analysis can not predict the critical condition for the second transition. The second transition was numerically simulated first by Muller et al and later Levenstam et al. But the second critical Marangoni number is not yet well understood. We have placed several simulations for Pr=0.01 and 0.02 and obtained the following results. Again, it should be noted that a two-dimensional simulation code always predicts steady solutions under any one of the following conditions. In the following simulations, the three dimensional perturbations has never been excited without adding very small random noise to velocity values at every mesh points. A set of randum values (average value = 0, standard deviation=10^{-8}) was generated at each time step and added to velocity values until the three dimensional perturbation grown up to the order of 10^{-3}, then quitted. Without these artificial velocity perturbations, no three dimensional flow was initiated. Temperature perturbations did not work at all.

6.1 Results with Pr=0.01

6.1.1 As=1.0 and Ma= 50

In this case, as shown in **Fig. 30** an axisymmetric flow field was established very quickly and the velocity and temperature distributions are indistinguishable from those given by the two-dimensional code. By continuous addition of small random noises on velocities, very weak (10^{-3}) three dimensional disturbance was incubated and started exponential growth with time. As the disturbance grow up to O(5×10^{-3}) at τ=20 , the surface velocities changed abruptly. The flow field indicated a quick transition to a three dimensional steady flow with a dominant azimuthal wave number m=2. The three dimensional flow maintained itself steady thereafter. The structure of the steady three dimensional flow and temperature fields are shown in **Fig. 31**. The growth rate constant β of the azimuthal velocity component at the monitoring point depends on the value of the exposed Marangoni number values as shown in **Fig.32**. By interpolating to β=0, the first critical Marangoni number is determined as Mac_1=20.8. for As=1.0 and Pr=0.01. The value is very good agreement with the result of linear stability analyses (Mac_1=19.0) and also of the nonlinear numerical simulation of Levenstam et al. They obtained Mac_1= 19.6, by means of a three dimensional finite element code. The origin of the 3D flow is not the temperature gradient in azimuthal direction. There are many controversial flow on the surface; surface fluid flows toward hotter spot.

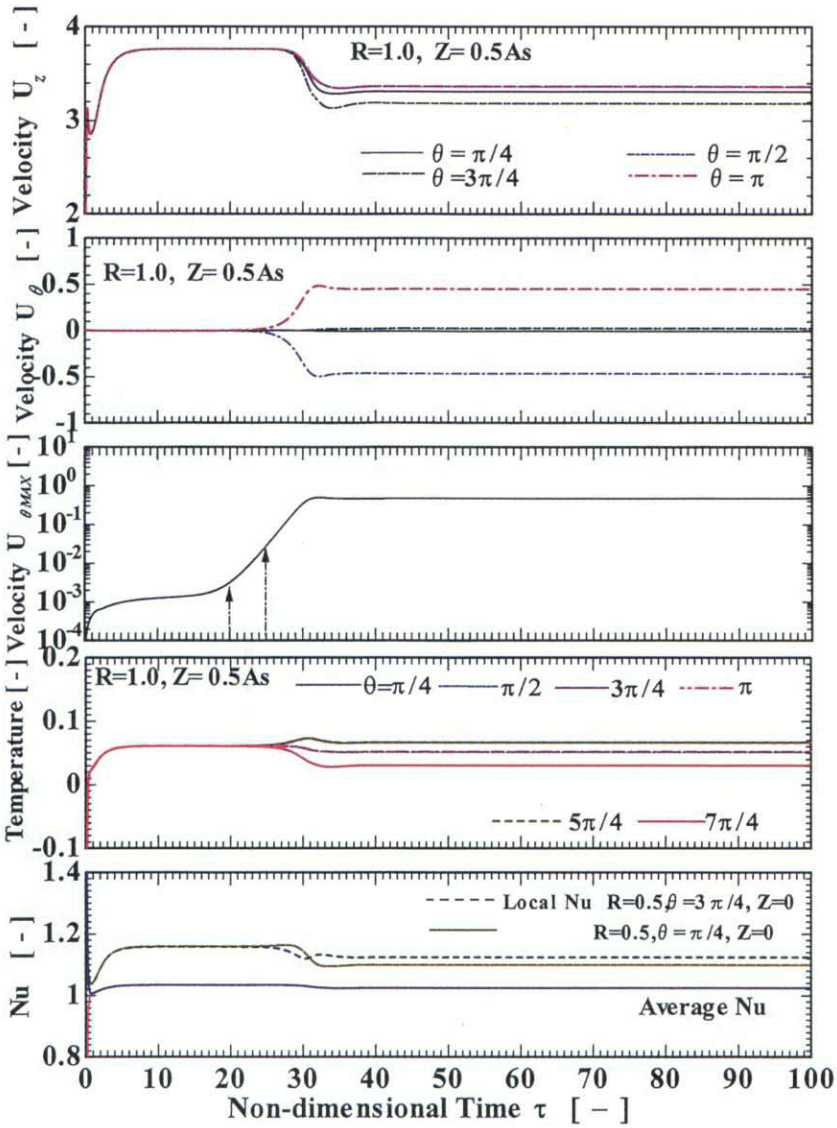

Fig.30 Time evolution of 3D steady Marangoni flow at Ma=50, Pr=0.01 and As=1.0.

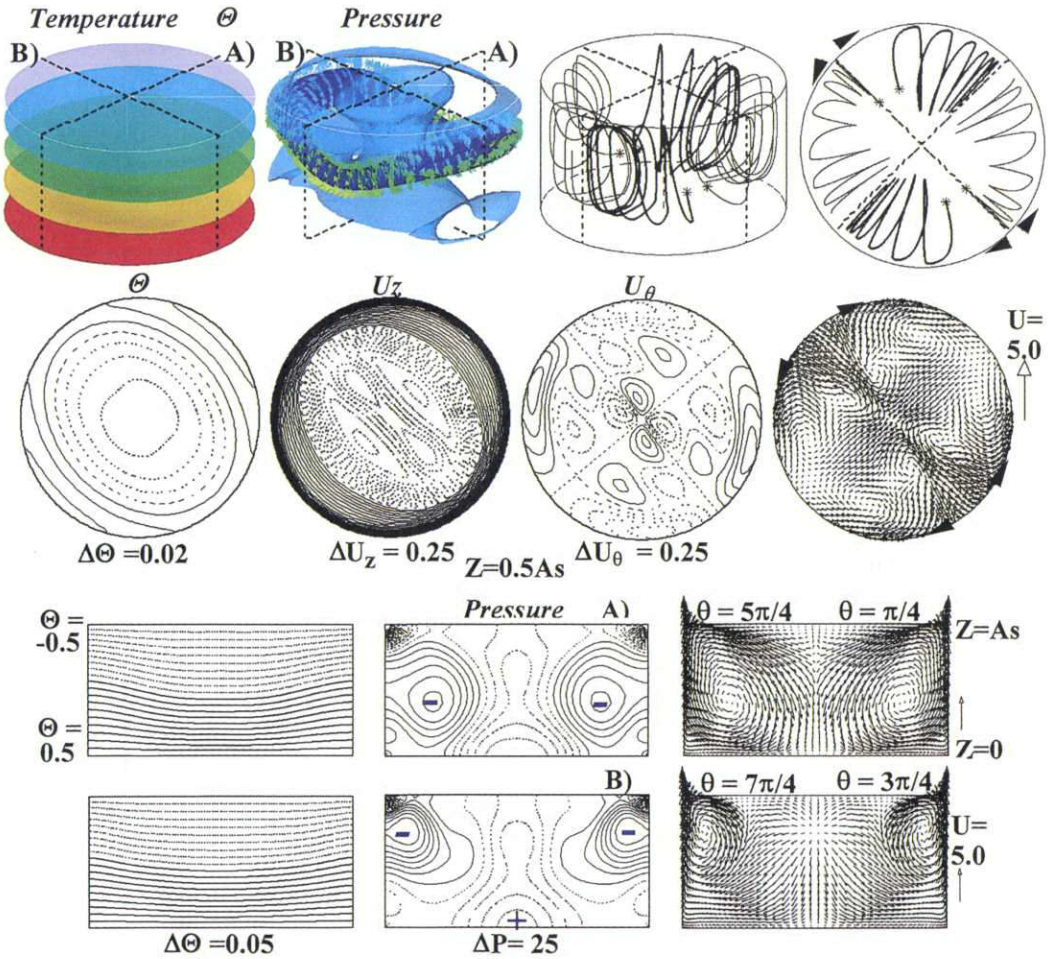

Fig.31 Structure of velocity and temperature fields in a steady 3D Marangoni flow: Ma=50, Pr=0.01 and As=1.0.

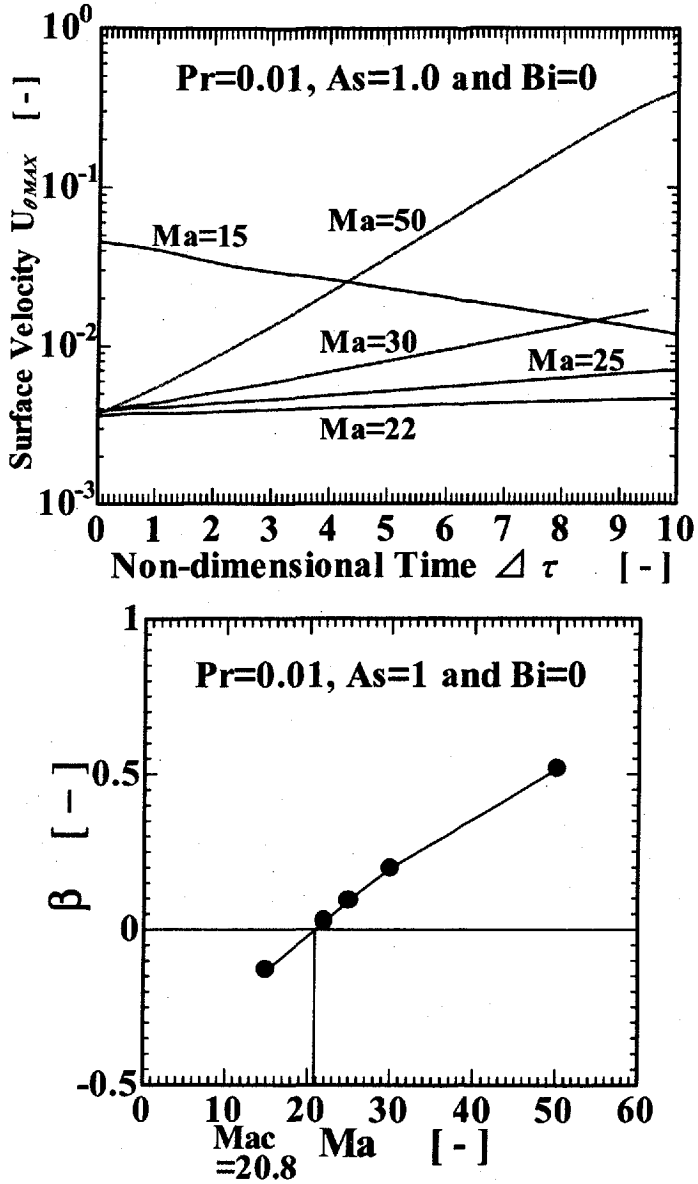

Fig.32 Growth rate constant constant, β, of the maximum value of azimuthal velocity as a function of the Marangoni number. The first critical Marangoni number is determined by interpolating to β=0.

6.1.2 As=1.0 and Ma= 90

In this case, after initial transient period, pseudo steady m=2 flow field was once established. But this flow field is unstable against 3D disturbances of odd azimuthal wave numbers (m=1, 3…). **Fig. 33** indicates that a time dependent disturbance of m=1, or odd disturbances, superoposes onto the steady 3D structure and generates the oscillatory 3D Marangoni flow throughout the liquid bridge. The basic 3D steady flow maintains itself stationary. The strength of the superposed disturbances show spacio-temporal variation, then the 3D flow field start oscillation. The origin of the 3D disturbances in low Prandtl number fluids are, as has been pointed out by Dr. Kuhlmann in this research group, inertia and hydrodynamic instabilities in the thin shear layer which appears near the axis. The periodic oscillatory disturbances grow up from very small disturbances expomentially with time. By plotting the growth rate constant against Ma, we get **Fig.34** and the second critical Marangoni number is determined by interpolating to β=0. Thus determined Mac_2 is 66.5 with ω_c= 0.765. These are comparable to Mac_2=62.5 reported by Levenstam and Amberd [13] by means of finite element method. This suggests the numerical code is reasonably accurate.

6.2 Results with Pr=0.02

The code was also applied to a different configurations. Here, we conducted a simulation with Pr=0.02. The first critical Marangoni number in As=1.0 liquid bridge is determined Mac_1 =34.8, which is very close to the Mac_1 =34.3 predicted by linear stability analysis.

A second series of simulations for As=1.80 was conducted. The first critical Marangoni number is determined Mac_1=21.4, which is also comparable to Mac_1=20.6 predicted by linear stability analysis. The flow structure of the steady 3D flow is illustrated in **Fig.35.** In this case, as is expected, the dominant azimuthal wave number is m=1. The center of vortex draws a torus In Fig. 35, a iso-pressure surface indicated by dark blue color approximately represents the shape of the vortex core. The vortex core is extended in one direction and also slanted in the same direction. The trajectories of tracer particles explain the flow field. The trajectories indicate that the liquid bridge is practically divided into two independent segments by a vertical plane of mirror symmetry.

Further systematic simulations enabled us to determine the second critical Marangoni number Mac_2=61.6 and the critical frequency wc=3.08. There is no report available reference values on Mac_2 and ω_c for As=1.80.

Some of the numerical results have been visualized and recorded on Video Tape. The tape could be available upon request.

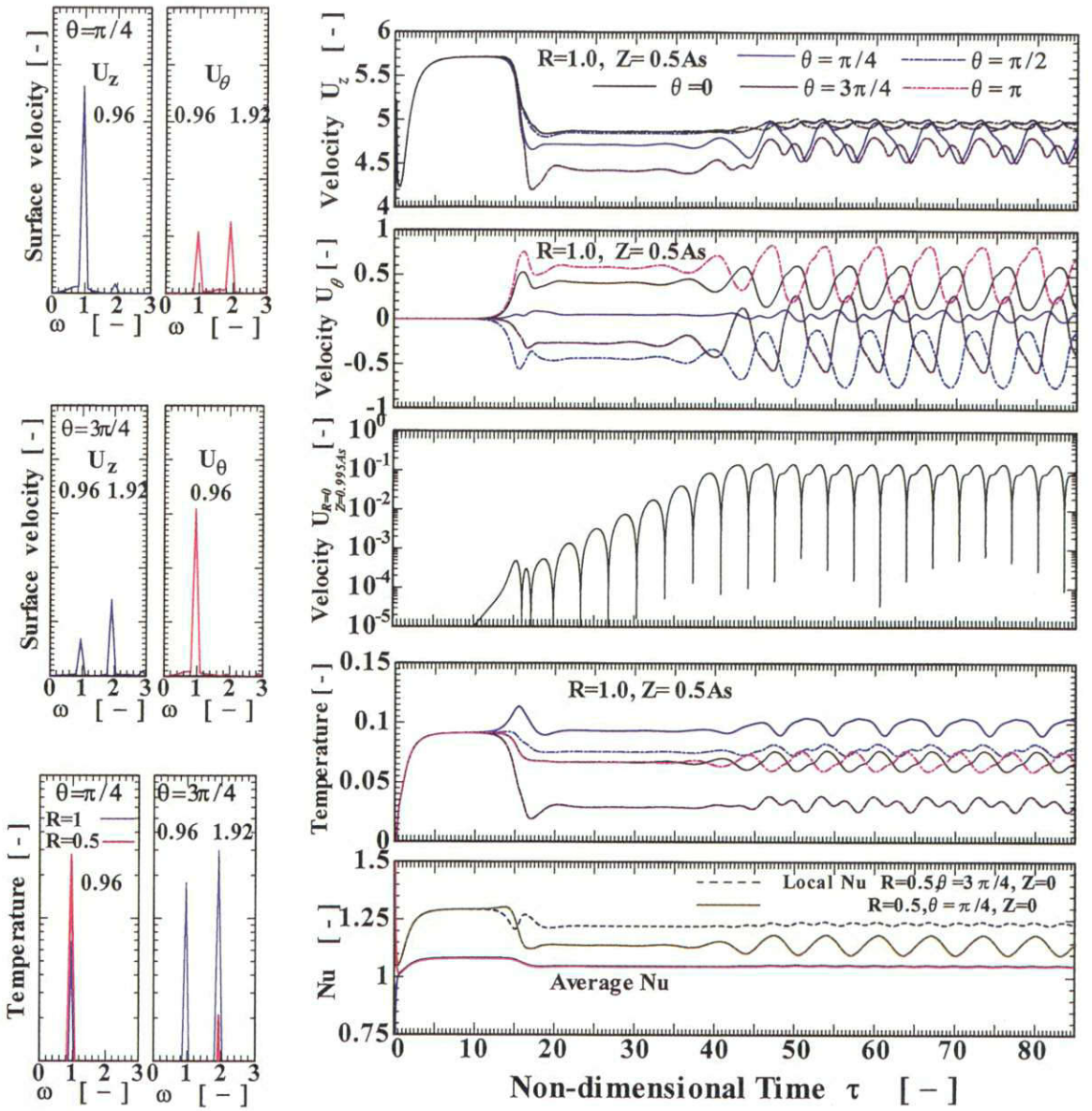

Fig.33 Temporal variations of an oscillatory 3D Marangoni flow : Ma=90, As=1.0 and Pr=0.01.

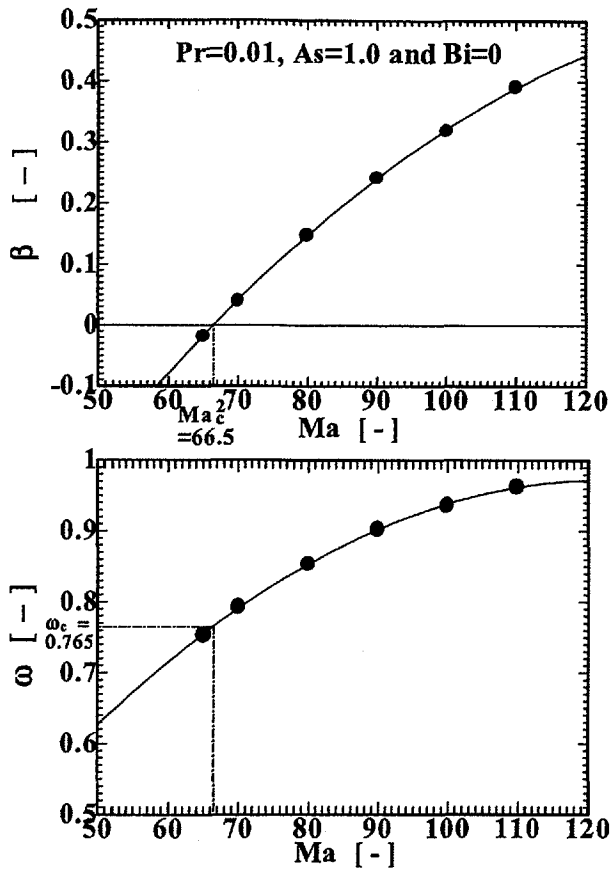

Fig.34 Growth rate constant for the amplitude of U_θ as a function of Ma: As=1.0, Pr=0.01

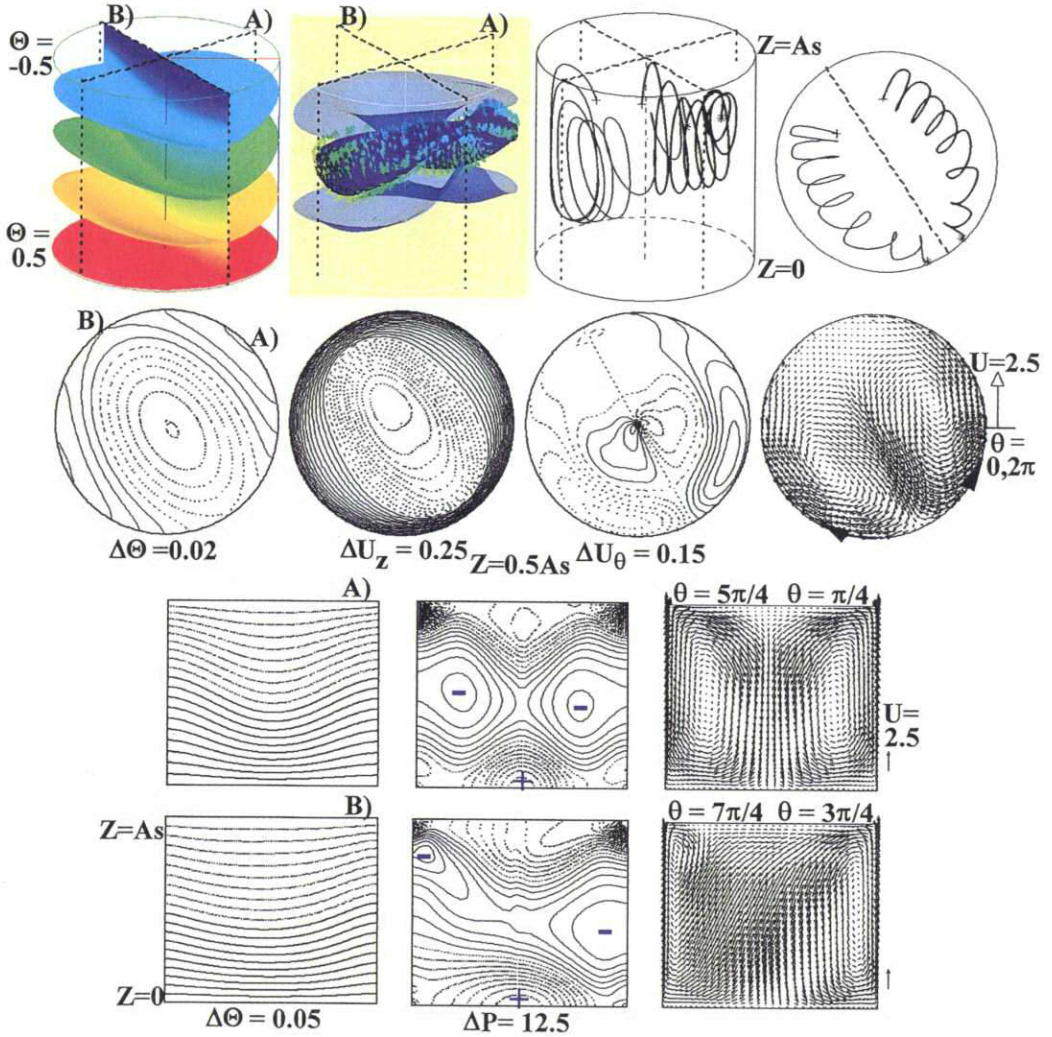

Fig.35 Structure of velocity and temperature fields in a steady 3D Marangoni flow in a long liquid bridge : Ma=50, Pr=0.02 and As=1.8.

7 Conclusion

From the present three-dimensional simulations, we obtained the following conclusion.

1) Three-dimensional oscillatory flows were self-excited even with the errors of numerical calculations. In this series of simulations with As=0.75, 1.0, 1.33 and 1.60, the azimuthal wave number m ranged from 1 to 4 explaining the well-known multi-morphological feature of the 3-D oscillatory Marangoni flow in half-zones. In most cases studied here, the initially grown disturbances exhibited pulsating oscillation. At large Marangoni numbers, the pulsating oscillation became unstable and often exhibited transition to rotating type oscillation. However, *pulsating* oscillations were incubated and remained for very long time span with m=4 at As= 0.75, Ma=7770, and with m=2 at As=1.6, Ma=4440.

2) 3-D disturbances with small oscillation amplitude grow or decay exponentially with time. The present simulations clarified the order of magnitude of the growth rate constant β as a function of Ma as shown in Fig.27.

3) The critical Marangoni numbers were determined. The critical Marangoni numbers are very close to those of the linear stability analysis within few per cent of error. The largest deviation (about 8%) occurred at As=0.75 where the present simulation was least reliable because of the insufficient resolution.

4) The azimuthal wave number m of the most dangerous mode is roughly approximated by an expression, m=2/As. But at super critical conditions (Ma/Ma_c>1), disturbances with m other than the most dangerous mode were excited. These indicate the validity of the mode selection rule proposed in the previous paper, i.e., a disturbance which shows the largest growth rate constant at a given condition becomes dominant.

5) Growth rate constants were correlated as a function of the reduced Marangoni number. Assuming the correlation to be the case for wide range of Marangoni number, we concluded that the apparent critical Marangoni number is very strongly dependent on both the liquid bridge size and length of observation time.

6) The numerical code was applicable to low Prandtl number fluids. The code and the results gave us first critical Marangoni numbers for different configurations. These values fall very close to the linear stability analysis and previous non-linear simulations.

7) Perspective views of 3D flow structure were visualized and represented on hard copies and also recorded on video tape. These would help understandings of the complex phenomena.

REFERENCES

1)Schwabe, D., Scharmann, A., "Some evidence for the existence and magnitude of a critical Marangoni number for the one set of oscillatory flow in crystal growth melt.", *J. Crystal Growth*, **46**, 125 (1979).

2)Preisser, F., Schwabe, D., Scharmann, A., "Steady and oscillatory thermocapillary convection in liquid columns with free cylindrical surface", *J. Fluid Mech.*, **126**, 545 (1983)

3)Velten, R., Schwabe, D., Scharmann, A., "The periodic instability of thermocapillary convection in cylindrical liquid bridges", *Phys. Fluids*, A**3**, 267 (1991)

4)Carotenuto, L., Albanese, C., Castagnolo, D., Monti, R., in: Ratke, L., Walter, H., Feuerbacher, B.(eds.), "Materials and fluids under low gravity", Berlin; Springer; 331 (1996)

5)Kamotani, Y., Ostrach, S., Vargas, M., "Oscillatory thermocapillary convection in a simulated floating-zone configuration", *J. Crystal Growth*, **66**, 83 (1984)

6)Schwabe, D., Hintze, P., Frank, S., "New features of thermocapillary convection in floating zones revealed by tracer particle accumulation structures(PAS)", *Microgravity sci. techn.*, **9**, 163 (1996)

7) Nakamura, S., Hibiya, T., Kakimoto, K., Imaishi, N., Nishizawa, S., Hirata, A., Mukai, K., Yoda, S., and Morita, T.S., "Temperature fluctuations of the Marangoni flow in a liquid bridge of molten silicon under microgravity on board the TR1-A-4 rocket", *J. Crystal Growth*, **186**, 85(1998)

8)Rupp, R., Muller, G., Neumann, G., "Three dimensional time dependent modeling of the Marangoni convection in zone melting configurations for GaAs" , *J. Crystal Growth* , **97**, 34(1989)

9)Neitzel, G.P., Law, C.C., Jankowski, D.F., Mittelmann, H.D., " Energy stability of thermocapillary convection in a model of the float-zone crystal-growth process. 2: Non-axisymmetric disturbance", *Phys. Fluids*, A**3**, 2841 (1991)

10)Neitzel, G.P., Chang, K.T., Law, C.C., Jankowski, D.F., Mittelmann, H.D., "Linear stability theory of thermo-capillary convection in a model of the float-zone crystal growth process" , *Phys. Fluids*, A**5**, 108 (1993)

11)Wanschura, M., Shevtsova, V.M., Kuhlmann, H.C., Rath, H.J., "Convective instability mechanisms in thermocapillary liquid bridges", *Phys. Fluids*, A**7**, 912 (1995)

12)Chen, G., Liz, F. A., Roux, B., "Bifurcation analysis of the thermocapillary convection in cylindrical liquid bridge", *J. Crystal Growth*, **180**, 638 (1997).

13)Levenstam, M., Ambrg, G., "Hydrodynamical instabilities of thermocapillary flow in a half-zone", *J. Fluid Mech.*, **297**, 357 (1995).

14)Savino, R., Monti, R., "Oscillatory Marangoni convection in cylindrical liquid bridge", *Phys.of Fluids*, **8**, 2906 (1996)

15)Imaishi, N., Yasuhiro, S., "Numerical simulation of three dimensional unsteady Marangoni convection in Half-zone", *Proc. 2nd Europ. Symp. Fluids in Space*, p.67 (1996)

16) Yasuhiro, S., Sato, T., Imaishi, N.,"Three dimensional oscillatory Marangoni flow in half-zone of Pr=1.02 fluid.", *Microgravity sci. techn.*, **11**, 1 (1998)

17)Castagnolo, D., Carotenuto, L., "A numerical simulation of three dimensional thermocapillary flows in liquid bridges", *Physics of Fluids*, to appear

18)Suzuki, T., Kawamura, H., "Consistency of finite-difference scheme in direct numerical simulation

of turbulence", *J. Mech. Eng. Japan (in Japanese)*, **60**-578(B), 58 (1994)

19)Ozoe, H., Toh, K., "Dopant concentration profile in a Czochralski flow of liquid metal in a vertical or horizontal magnetic field", *J. Crystal Growth*, **130**, 645 (1993).

20)Hirt, C. W., Nichols, B. D., Romero, N. C., "SOLA - A Numerical Scientific Algorithm for Transient Fluid Flow", *Los Alamos Scientific Laboratory*, LA-5852 (1975)

21)Kuhlmann, H. C. and Rath, H. J., "On the interpretation of phase measurements of oscillatory thermocapillary convection in liquid", *Phys. Fluids* , A**5**, 2117 (1993)

22)Yasuhiro, S., Sato, T., Imaishi, N., Kuhlmann, H.C., "Growth rate of three dimensional oscillatory Marangoni flow in liquid bridge of Pr=1.02 fluid", submitted to Physics of Fluid

23) Y. Ar, Z.M. Tang, J.H. Han, Q. Kang, and W.R. Hu, The measurement of azimuthal velocity field for oscillatory thermocapillary convection of floating half zone, *Microgravity sci. and techn.*, **10**, 129 (1998)

24) L. Carotenuto, D. Castagnolo, C. Albanese, and R. Monti, 1998, "Instability of thermocapillary convection in liquid", *Physics of Fluids*, **10**, 555 (1998)

25) J. Masud, Y. Kamotani, and S. Ostrach, "Oscillatory thermocapillary flow in cylindrical columns of high Prandtl number fluids", *J. Thermophysics Heat Transfer*, **11**, 105 (1997)